BOREAS An international journal of Quaternary research

Reconstructing the Holocene glacial history of northern Troms and western Finnmark, Arctic Norway

JOSH R. LEIGH, RICHARD S. JONES, CHRIS R. STOKES, DAVID J. A. EVANS, J. RACHEL CARR AND LISS M. ANDREASSEN

BOREAS

Leigh, J. R., Jones, R. S., Stokes, C. R., Evans, D. J. A., Carr, J. R. & Andreassen, L. M.: Reconstructing the Holocene glacial history of northern Troms and western Finnmark, Arctic Norway. *Boreas*. https://doi.org/10.1111/bor.12668. ISSN 0300-9483.

Here we present the first Lateglacial and Holocene glacial history from Rotsunddalen, northern Troms and western Finnmark county, northern Norway, based on both relative and numerical moraine dating using Schmidt hammer, soil chronosequencing and terrestrial cosmogenic nuclide dating. We combine these chronological data with a regional map of the glacial geomorphology to hypothesize key events in the glacial history from around 14 ka to present. Our reconstruction shows that, following deglaciation of the main ice sheet across central Troms and Finnmark, mountain glaciers were terminating on land, close to the coast, between around 12.1 and 10.6 ka. Continued recession of the main Fennoscandian Ice Sheet margin towards the SE led to the isolation of several large plateau icefields and outlet glaciers that generated moraines at around 10.2–9.2 ka, which we ascribe to the Erdalen Event, and 8.4–8.2 ka, which is broadly contemporaneous with the 8.2 ka cold event. Although the latter corresponds with the Scandinavian Finse Event, very few moraines have been dated to this time and we therefore view it as a tentative hypothesis for future work to test. During the Holocene Thermal Maximum (~6.6 to 6.3 ka) most (if not all) glaciers in the region disappeared, but then regrew during the Neoglaciation and produced large moraines dated to around 4.7 ka that lie a few hundred metres distal to the prominent Little Ice Age moraines (previously dated to AD 1810s–1870s). Given the limitations of our dating approach, the preservation of moraines dated to this period in northern Norway also warrants further investigation. We also highlight that terrestrial cosmogenic nuclide dating of the moraines is not consistent with other dating approaches and the widely established deglaciation history of the region, probably owing to cosmogenic inheritance and insufficient glacial erosion.

Josh R. Leigh, Chris R. Stokes (corresponding author: c.r.stokes@durham.ac.uk) and David J. A. Evans, Department of Geography, Durham University, South Road, Durham DH1 3LE, UK; Richard S. Jones, School of Earth, Atmosphere and Environment, Monash University, 9 Rainforest Walk, Clayton, Victoria 3800, Australia; J. Rachel Carr, School of Geography, Politics and Sociology, Newcastle University, Henry Daysh Building, Newcastle upon Tyne NE1 7RU, UK; Liss M. Andreassen, Norwegian Water Resources and Energy Directorate (NVE), Postboks 5091, Majorstua, 0301 Oslo, Norway; *received 11th September 2023, accepted 14th May 2024.*

Glaciers are highly sensitive to climatic perturbations and reconstructions of their former extent are important to improve our understanding of climate variability (Oerlemans 2005; Nesje *et al*. 2008; Wittmeier *et al*. 2015; Roe *et al*. 2017). In northern Norway, numerous studies have demonstrated a clear response of glaciers to even short-lived climatic fluctuations (Bakke *et al*. 2005b; Oerlemans 2007; Andreassen *et al*. 2012a, b; Stokes *et al*. 2018; Leigh *et al*. 2020; Weber *et al*. 2020). The high sensitivity of these glaciers is predominantly due to their maritime location and response to multi-decadal variations in the Arctic Oscillation and North Atlantic Oscillation (Nesje *et al*. 2000, 2008). Furthermore, observational data and numerical modelling both indicate an increased sensitivity to global climate change in the Arctic (Serreze & Barry 2011; Park *et al*. 2019). The resulting amplification of Arctic climate change is characterized by substantial regional disparity in temperatures between southern and northern Norway (Ballantyne 1990; Bjune *et al*. 2005; Paasche *et al*. 2007).

Given concerns over the future decline of glaciers in northern Norway (Nesje *et al*. 2008; Rounce *et al*. 2023), it is important to contextualize recent changes in a longer-term context and constrain their response to major circum-Arctic climate events since the Lateglacial and through the Holocene e.g. the Younger Dryas (YD), the 8.2 ka event, the Holocene Thermal Maximum (HTM), and the Little Ice Age (LIA) (e.g. Nesje 2009; Tanarro *et al*. 2021). However, research constraining the age and magnitude of glacier fluctuations across Scandinavia during this period is generally focused on the larger ice caps and outlet glaciers in southern regions (cf. Nesje *et al*. 2008; Nesje 2009). In contrast, most previous work in northern Norway has focussed on the retreat of the main Fennoscandian Ice Sheet from the outer to inner fjord areas and onto the mainland (Andersen 1968; Sollid *et al*. 1973; Corner 1980). These studies used extensive mapping of fjord moraine successions and raised shorelines, coupled with radiocarbon dating, to build up a picture of ice-front positions (e.g. Holmes & Andersen 1964; Andersen 1968; Sollid *et al*. 1973; Corner 1980) and, more recently, retreat rates (Stokes *et al*. 2014). However, the short-lived and less extensive glacier fluctuations during the Holocene have been largely overlooked. For example, large scale ice-sheet reconstructions (Hughes *et al*. 2016; Stroeven *et al*. 2016) that have mapped the retreat of the Fennoscandian Ice Sheet from its maximum position at

DOI 10.1111/bor.12668

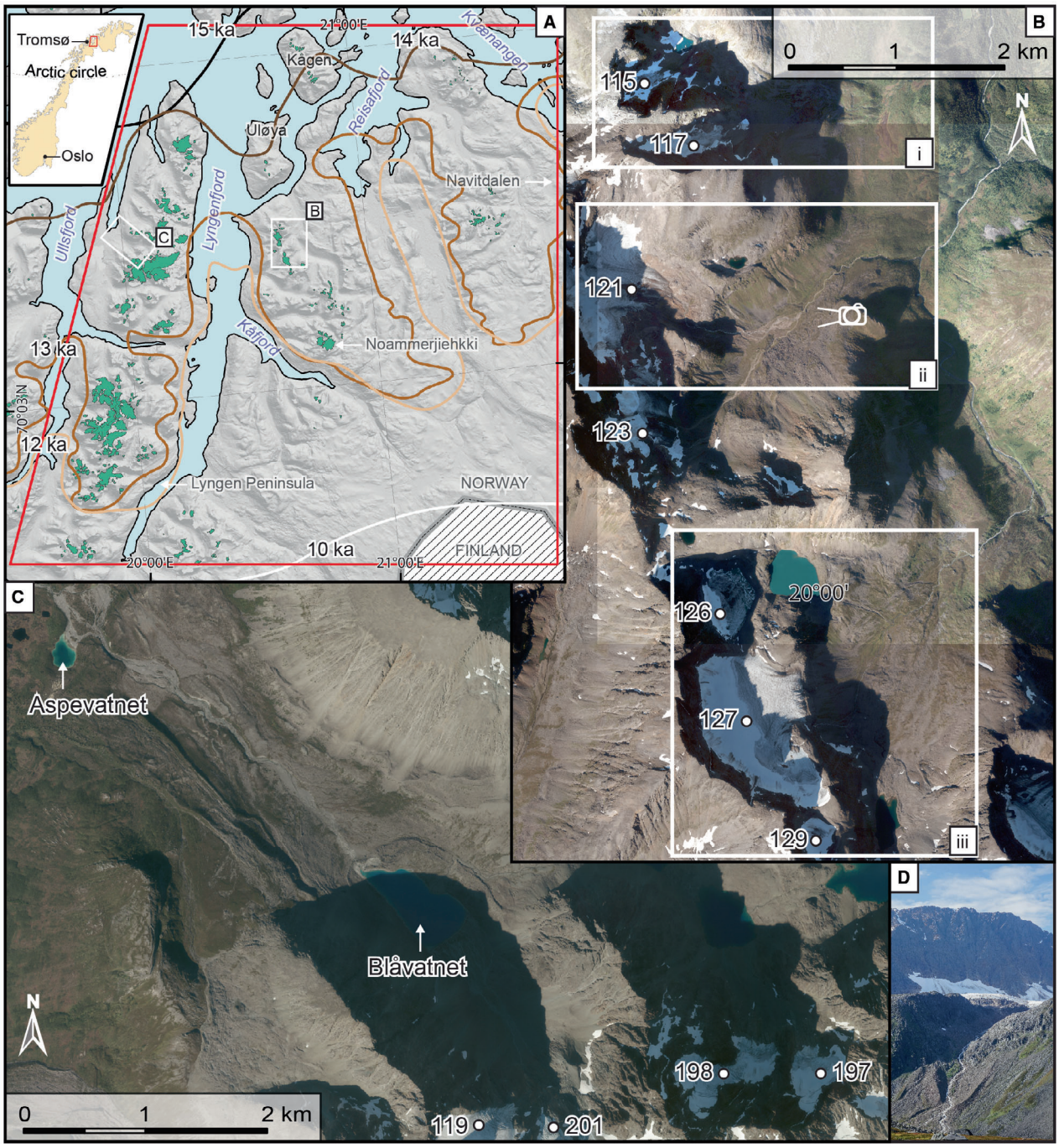

Fig. 1. A. Study area (red outline) in Troms and Finnmark county, northern Norway, together with Fennoscandian Ice Sheet margins from Hughes *et al.* (2016) at 15, 14, 13, 12, 11, and 10 ka (thousands of years ago). The two field sites are shown as white rectangles: (B) Rotsunddalen and (C) Strupskardet. Rotsunddalen (B) has three subsidiary valleys: Hjemtverrdalen (i), Sorbmevággi (ii), and Goahtevággi (iii). The camera in (ii) denotes the location of the photograph in (D), which is a field photograph (27 August 2019) of the LIA moraines in front of glacier 121 (glacier numbers refer to those in the Norwegian Glacier Inventory: Andreassen *et al.* 2012b). The base image in (A) is a hill-shaded Arctic digital elevation model (DEM) mosaic with present-day glaciers marked in green, and the images in (B) and (C) are 0.25 cm resolution aerial orthophotographs captured on 24 August 2016, from www.norgeibilder.no.

the continental shelf (~22 to 21 ka), to the Norwegian coastal margin around 16 ka, through the fjords at ~13 to 12 ka, and its final deglaciation towards the south and east by around 10 ka (Fig. 1A), do not resolve smaller scale fluctuations of mountain glaciers and ice caps. Indeed, only a handful of studies have investigated the Holocene history of smaller mountain glaciers and ice caps in the region (e.g. Ballantyne 1990; Bakke

et al. 2005b; Wittmeier et al. 2015) and their retreat since the LIA (e.g. Stokes et al. 2018; Leigh et al. 2020). Thus, an improved understanding of the fluctuations of mountain glaciers in northern Norway throughout the Holocene is required to: (i) assess the asynchronicity of glacier response across a latitudinal gradient that crosses the Arctic Circle; (ii) translate the effects of historic rapid climatic fluctuations into local glacier response; and (iii) help local communities adapt and prepare for future changes in glacier extent.

The aim of this paper is to reconstruct the glacial history of central Troms and Finnmark county, northern Norway, during and since the recession of the Fennoscandian Ice Sheet from around 14 ka to the present. We do this by combining a previously published glacial map of the region (Leigh et al. 2021), with both relative and numerical age dating of moraines in Rotsunddalen (the Rotsund Valley) in the Kåfjord Alps. Ages are given as calendar/calibrated ages (ka), unless otherwise stated.

Previous work and study area

Holocene glacier activity in Troms and Finnmark

Following deglaciation of the Fennoscandia Ice Sheet from its Last Glacial Maximum (*c*. 22–10 ka; Hughes et al. 2016; Stroeven et al. 2016), glaciers and ice caps in Norway are thought to have undergone a complex pattern of retreat and readvance throughout the Holocene (Nesje et al. 2008; Nesje 2009). The most notable of these climatically driven fluctuations are: (i) the readvance/stillstand during the Erdalen Event around 10.1–9.7 ka (e.g. Dahl et al. 2002; Matthews et al. 2008); (ii) the 8.2 ka cold event (correlative with the Finse Event in southern Norway, e.g. Nesje & Dahl 2001); (iii) the HTM of around 8–6 ka (e.g. Bjune et al. 2005; Renssen et al. 2012); (iv) short periods of increased glacier activity after the regional onset of the Neoglaciation around 6–2 ka (e.g. Matthews & Dresser 2008); (v) the LIA that culminated between AD 1300 and the early 1900s (e.g. Grove 2004); and (vi) the rapid recession to the present-day (post 1980s) owing to anthropogenically forced climate change (e.g. Andreassen et al. 2012a; Stokes et al. 2018; Leigh et al. 2020).

A period of cooling during the Early-Holocene transition from Preboreal to Boreal, subsequently termed the Erdalen Event (10.1–9.7 ka; Dahl et al. 2002; Matthews et al. 2008), is evidenced across Norway by substantial moraines inset within the YD limits (Andersen 1980; Corner 1980; Nesje & Kvamme 1991; Dahl et al. 2002; Turner & Marshall 2011; Jansen et al. 2023). It is also recorded in environmental records from non-glacial sites, such as vegetation regression linked to decreased summer temperatures (Paus et al. 2006, 2019). Erdalen Event moraines are often grouped into two or three major zones, thought to have formed between 10.1 and 9.5 ka (e.g. Andersen 1980; Nesje et al. 1991; Dahl et al. 2002; Bakke et al. 2005a; Matthews et al. 2008; Aa & Sønstegaard 2019). In the Lyngen region of northern Norway, adjacent to the study area, Ballantyne (1990) noted the presence of probably Preboreal moraines and Bakke et al. (2005b) have identified three closely grouped moraines formed during the period from 10.4 to 8.9 ka. On the Bergfjord Peninsula (~70 km NE of Lyngenfjord), reconstructions of the Holocene history of the Langfjordjøkelen ice cap do not, however, record the same pattern of advance as those described in the Lyngen region. Rather, Wittmeier et al. (2015) concluded that between 10.0 and 4.1 ka, the northern outlet glacier of Langfjordjøkelen was absent or too small to contribute minerogenic deposits to its proglacial lakes (Wittmeier et al. 2015).

Over the period from 10 to 6 ka, the Holocene climate was steadily warming (Turner & Marshall 2011) but was interrupted at around 8.2 ka by an abrupt, short-lived period of cooling (Alley et al. 1997; Rohling & Pälike 2005). This 8.2 ka event is often known as, and/or incorporated within, the Scandinavian Finse Event (Dahl & Nesje 1994, 1996; Nesje & Dahl 2001; Nesje et al. 2008; Nesje 2009; Aa & Sønstegaard 2019). Few studies have attributed specific moraines to the 8.2 ka climatic deterioration across Norway and/or found evidence for substantial readvance and possible regrowth of ice caps and mountain glaciers. Instead, the event is more typically recorded in pro-glacial lake sediments that indicate glacier-derived sediments prior to a period of warming in the Middle Holocene (Nesje & Dahl 2001; Seierstad et al. 2002; Nesje et al. 2006, 2008; Nesje 2009; Gjerde et al. 2016; Aa & Sønstegaard 2019).

Following the 8.2 ka event, the warming during the Middle Holocene is referred to as the HTM, during which summer temperatures are thought to have been between 1.5 and 2 °C higher than at the 20th/21st century boundary (Bjune et al. 2005; Nesje et al. 2008; Nesje 2009). Across Scandinavia, the peak of the HTM is thought to have occurred between 6.6 and 6.3 ka, when most glaciers are thought to have disappeared completely (Seppä & Birks 2002; Bjune et al. 2005; Seppä et al. 2005; Nesje et al. 2008; Nesje 2009; Renssen et al. 2009, 2012). For example, on the Lyngen Peninsula, northern Norway, no glacier-derived meltwater sediments are found in the Strupskardet proglacial lake between 8.8 and 3.8 ka, indicating a fully deglaciated catchment, and with equilibrium-line altitudes (ELAs) estimated to be above 1200 m a.s.l. (Bakke et al. 2005b; Wittmeier et al. 2015).

The HTM was followed by a gradual period of cooling from around 6–2 ka, which resulted in glaciers reforming across Scandinavia and culminating in the Neoglaciation (Grove 2004; Nesje et al. 2008; Nesje 2009; Wittmeier et al. 2015). Across Norway there is an apparently heterogeneous growth of glaciers during the Neoglaciation, with the development of glaciers responding to regional variations in winter precipitation, summer temperature, wind drift of snow and glacier hypsometry

(Nesje 2009). For example, valley glaciers on the Lyngen Peninsula are proposed to have reformed after around 3.8 ka (Bakke *et al.* 2005b); the Høgtuvbreen ice cap in the Svartisen area of northern Norway experienced initiation around 4.4–4.3 ka (Jansen *et al.* 2016); and cirque glaciers in Rondane, southern Norway, regrew around 4 ka (Kvisvik *et al.* 2015). Throughout the Neoglaciation, proglacial sediments record a series of events during which glaciers were larger than they are at the present day and, in some cases, beyond their most recent LIA maxima (e.g. Matthews *et al.* 2005; Matthews & Dresser 2008; Bakke *et al.* 2010; Wittmeier *et al.* 2015). However, in most cases, it is generally considered that the culmination of the Norwegian Neoglaciation occurred during the LIA (Nesje 2009).

Initiating at around AD 1300, glaciers in the Northern Hemisphere underwent a pattern of asynchronous readvance, with multiple major LIA advances in the following few centuries (Grove 2001, 2004). Unlike in continental Europe, which experienced relatively uniform LIA maxima during the mid-19th century, glaciers in Norway showed considerable regional asynchronicity in the extent and timing of the LIA maximum, from the mid-18th century in southern Norway to the early 20th century in northern Norway (Ballantyne 1990; Grove 2001, 2004; Winkler 2003; Ivy-Ochs *et al.* 2009; Solomina *et al.* 2016; Leigh *et al.* 2020). Regional differences in LIA maxima across Norway appear to be influenced primarily by differences in summer temperature and winter precipitation, with local scale differences being explained, in part, by individual glacier hypsometry (e.g. Ballantyne 1990; Nesje *et al.* 2008; Leigh *et al.* 2020). For example, Ballantyne (1990) noted that, on Lyngen, all glaciers exceeded or nearly exceeded their mid-18th-century maxima in 1910–1930, whereas the mid-18th-century advance was generally much more extensive than any early-20th-century advance in southern Norway. He argued that this might be explained by a southerly migration of the North Atlantic oceanic polar front in the mid-18th century, which resulted in a reduction in precipitation over northern Norway, but an increase over southern Norway.

Since the culmination of the LIA, most glaciers across Norway (and globally) have experienced net mass loss (e.g. Nesje *et al.* 2008; Andreassen *et al.* 2012a; Zemp *et al.* 2015). Observations of glacier change since the mid-20th century show exceptionally rapid retreat, primarily linked to anthropogenically forced climate change (e.g. Stokes *et al.* 2018; Zemp *et al.* 2015, 2019; Leigh *et al.* 2020). Furthermore, a recent synthesis of changes in glacier area, length, surface elevation, and mass balance of glaciers in mainland Norway revealed that those in the northernmost counties (i.e. Troms and Finnmark) showed no sign of advance in the 1990s, as found for glaciers further south, and that the mass deficits were largest for the northern-most monitored glacier Langfjordjøkelen (Andreassen *et al.* 2020). Arctic Amplification is also likely to further impact glaciers in northern Norway, many of which may disappear before the end of the 21st century (e.g. Nesje *et al.* 2008; Stokes *et al.* 2018; Zemp *et al.* 2019; Leigh *et al.* 2020; Rounce *et al.* 2023).

Study area

The study area covers 6810 km^2 of Troms and Finnmark county, extending from the Lyngen Peninsula in the west to Navitdalen in the east, and including the small islands of Uløya and Kågen in the north (Fig. 1). Most glaciers in the region can be broadly considered maritime given their proximity to large fjord systems and the North Atlantic Ocean. There are no continuous, long-term meteorological records in the study area, with the nearest stations in the city of Tromsø, located around 60 km to the west (station number 90450) and at Karasjok, located around 200 km to the east (station number 97350). For reference, mean January and July temperatures in Tromsø (1995–2018) are −3.1 and +12.3 °C, respectively; whereas they are −13.6 and +13.4 °C at Karasjok over the same period (Leigh *et al.* 2020). Total annual precipitation at Tromsø (1995–2018) is 1076 mm, whereas it is 430 mm at Karasjok (https://selkima.met.no). Thus, present-day glaciers are exposed to relatively high precipitation during the winter, but with a smaller amount than further west, and with a smaller range between winter and summer temperatures than for glaciers at similar latitudes further east (Andreassen *et al.* 2012b). Leigh *et al.* (2020) also reported a clear increase in mean annual temperature (of around 1.1 °C) since the 1980s, and that winter and summer precipitation had shown a steady decrease since the early 2000s. As a result, Leigh *et al.* (2020) found that the total area of glaciers within the study area had decreased by around 35 km^2 between 1989 and 2018 (n = 219 in 1989) and that very small glaciers (<0.5 km^2) showed the highest relative rates of shrinkage, such that 90% of mapped glaciers within the study area were less than 0.5 km^2 in 2018.

Two field sites currently characterized by small, valley and cirque glaciers were visited in August/September 2018 and 2019 to undertake geochronological investigations: Rotsunddalen (Fig. 1B) and Strupskardet (Fig. 1C). These study areas were chosen because previous glaciological investigations are sporadically spaced throughout the region and there have been fewer studies of how smaller mountain glaciers responded to Holocene climate variability.

Rotsunddalen. – Rotsunddalen (Fig. 1B) is situated within the Nordreisa Municipality and is flanked on the west by a minor mountain range (the Kåfjord Alps). The mountain peaks in this area range from 1077 m a.s.l. (Stortinden) to 1320 m a.s.l. (Geaippilvarri) and the bedrock is composed of Vaddas Nappe and Kåfjord

Nappe, broadly comprising metamorphic facies of amphibolite, quartzite, gneiss, and schist (Lindahl *et al.* 2005; Augland *et al.* 2014; Geological Survey of Norway 2015). The present-day tree line extends to ~400 m a.s.l. and, above this, alpine tundra is the dominant vegetation. To the west is a major fjord system, Lyngenfjord, and there are also subsidiary fjords to the north (Rotsundet) and south (Kåfjorden; Fig. 1).

Within Rotsunddalen, three subsidiary valleys were investigated to develop a preliminary chronology that could inform the much broader regional-scale mapping compiled in Leigh *et al.* (2021): (i) a short un-named, west–east orientated valley (henceforth referred to as Hjemtverrdalen; Fig. 1Bi), containing present-day glaciers 115 and 117 (numbers refer to those in the Norwegian Glacier Inventory: Andreassen *et al.* 2012b) and drained by the river Hjemtverrelva; (ii) the SW–-NE-orientated valley Sorbmevággi (Fig. 1Bii), containing glaciers 121 (Sorbmejiehkki) and 123 and drained by the River Sorbmejohka; (iii) the SW–NE-orientated valley Goahtevággi (Fig. 1Biii), containing glaciers 126, 127 (Goahtejiehkki), 129, 131 and 132, and drained by the River Goahtejohka. All three valleys have large latero-frontal moraine systems, with the terminus positions of the outermost moraines extending into the main part of Rotsunddalen at elevations from ~140 to ~340 m a.s.l. LIA moraines are present in the forelands of glaciers 115, 117, 121, 123, and 126, and have previously been dated to between AD 1814 and 1877 (Leigh *et al.* 2020).

Strupskardet. – The valley Strupskardet (Fig. 1C), in the Lyngen municipality, is a west–east-orientated valley crossing the northern Lyngen Alps. The Lyngen Alps are situated on a ~70-km-long peninsula (Lyngen Peninsula), flanked by Lyngenfjord to the east and Ullsfjorden to the west. To the north and south of Strupskardet are mountains ranging from 1042 m a.s.l. (Nordre) to 1625 m a.s.l. (Lenangstindan), with bedrock composed of Lyngsfjellet nappe, comprising ophiolitic gabbro, and metamorphic facies that include amphibolite and schist (Randal 1971; Coker-Dewey *et al.* 2000; Augland *et al.* 2014). The present-day tree line extends to ~350 m a.s.l. as a dispersed and stunted tree cover. Within Strupskardet there are two glacier-fed lakes: Aspevatnet (0.4 km^2, 30 m a.s.l.) and Blåisvatnet (~0.3 km^2, 189 m a.s.l.). These lakes are fed by glaciers 119, 201 (Lenangsbreen), 198 and 197, and the river that feeds Aspevatnet is sourced by Blåisvatnet.

Importantly, previous research by Bakke *et al.* (2005b) has established ages for most moraines within Strupskardet. Moraine ages were determined from various landforms (e.g. moraines and former shorelines) and sediment cores from the proglacial lake Aspevatnet. The resultant glacial chronology for Strupskardet indicates that moraine ages span the past 20 ka (Bakke *et al.* 2005b). The ages of the pre-YD moraines are more uncertain (J. Bakke, pers. comm. 2021), but those from the YD moraines and younger are more reliable. The moraines enclosing lake Blåisvatnet (Fig. 1C) were proposed to have formed at 12.8–11.5 ka (M8) and 9.3–8.9 ka (M12) (Bakke *et al.* 2005b). Additionally, three inset moraines at Blåisvatnet's eastern margin (M10, M11 and M12; ~1.8 km from the present-day glacier front) were dated to 10.4–10.3, 9.8–9.4, and 9.3–8.9 ka, respectively (Bakke *et al.* 2005b). Following deposition of the M12 moraine, no additional moraines were formed until the LIA maximum moraine (M13) at around AD 1890–1928 (Bakke *et al.* 2005b).

Material and methods

Glacial geomorphological mapping and ice-margin reconstructions

We used a new glacial geomorphological map of the study area (Leigh *et al.* 2021) to identify key sites for fieldwork and to underpin our reconstruction of the glacial history. This mapping used high-resolution georectified orthophotographs (0.25 m pixel resolution; courtesy of The Norwegian Mapping Authority n.d.), medium-resolution 2018/19 multispectral satellite imagery (10 m pixel resolution Sentinel-2A imagery), and both 10 and 2 m digital elevation models (DEMs; courtesy of The Norwegian Mapping Authority (n.d.) and The Polar Geospatial Center (Porter *et al.* 2018), respectively).

Glacial landforms were identified and digitally mapped as either vector lines or polygons using ESRIs ArcGIS software. The geomorphological features mapped included moraines, ridges within areas of discrete debris accumulations (DDAs), flutings, eskers, irregular mounded terrain, lineations, glacially streamlined bedrock, possible glacially streamlined terrain, pronival ramparts, rock glaciers, and lithalsas. Mapping of glaciers and lakes was done using a semi-automated process on 2018/2019 multispectral satellite imagery with manual correction of mapped units (e.g. glaciers/lakes cast under shadow, glaciers obscured by debris, glaciers terminating in proglacial lakes or where snow patches were erroneously classified as glaciers) to produce the most up-to-date outlines as possible.

We used the glacial geomorphological map from Leigh *et al.* (2021) and our new chronological data (see below) to reassess, and in some cases modify, the broader-scale ice sheet outlines from the DATED-1 time-slice reconstruction (Hughes *et al.* 2016). The small number of existing dating controls throughout the study area were also utilized to help revise and update the ice-margin chronology. Any revisions to the ice margin chronology were guided by the mapping in Leigh *et al.* (2021) (e.g. of major moraine systems) and high-resolution topographic data from the 2-m-resolution Arctic DEM (Porter *et al.* 2018). The new reconstructions of

plateau-ice-cap and mountain-glacier extent followed the geomorphological mapping of Leigh *et al.* (2021) but were also guided by present-day glacier extent and our new age constraints from Rotsunddalen. Owing to the relatively sparse geomorphological signature on the mountain plateau surfaces relative to the valley systems, there was a greater amount of uncertainty in these areas.

Field and laboratory data collection and analysis

During fieldwork, three subsidiary valleys in Rotsunddalen (Hjemtverrdalen, Sorbmevággi, and Goahtevággi; Fig. 1B) were examined alongside one valley on the Lyngen Peninsula (Strupskardet: Fig. 1C).

In Rotsunddalen, Sorbmevággi hosts the most extensive, best preserved and easily accessible moraines. Therefore, this valley was chosen as the focus of our dating work and was used as the baseline for comparisons with the two adjacent valleys. Within Sorbmevággi there were five clearly defined moraines that led up to (but not including) the LIA moraine, which was previously dated to AD ~1822±39 (Leigh *et al.* 2020). All five pre-LIA moraines were sampled with the aim of establishing moraine formation ages. All moraines that were examined and discussed in the text are identified sequentially starting at M1, which denotes the furthest down-valley. For example, for SM1, the first letter indicates the valley name (S = Sorbmevággi), the second letter indicates the feature in question (M = Moraine) and the number indicates position in the sequence (1 = furthest down-valley/terminal moraine).

On all moraines, Schmidt hammer readings and soil profiles were recorded from the frontal and lateral portions, where possible. Additionally, samples were collected for terrestrial cosmogenic nuclide (TCN) dating from stable boulders on the Sorbmevággi moraines and a series of perched boulders on a bedrock lip above the SM5 moraine and within the main part of Rotsunddalen.

In Strupskardet (Fig. 1C) an extensive sequence of at least 13 moraines has been previously investigated and dated (M1–M13; Bakke *et al.* 2005b). Moraines that pertain to the YD/Holocene transition were the primary targets for sampling in the work presented in this paper (moraines M8–M12, ranging from approximately 12.8 to 8.9 ka; Bakke *et al.* 2005b) to enable a comparison with those deemed to be a similar age in Rotsunddalen. Schmidt hammer readings were prioritized at these well-defined, bouldery moraine ridges.

Schmidt hammer dating. – Measurements of rock-surface hardness were taken using a Novatest N-type Schmidt hammer, with a specified impact energy of 2.207 N m^{-1} (Matthews & Winkler 2022). A careful assessment of all boulders was carried out prior to sampling and only large, stable boulders located on or near moraine crests were sampled. A relatively large number of impacts is generally considered necessary in Schmidt-hammer dating to account for within- and between-boulder variability and site variability in rebound (*R*) values (Matthews & Winkler 2022). Although there is no universally applicable minimum sampling size, it has been noted that sampling a high number of boulders with one or a few impacts is generally more representative than sampling fewer boulders with many impacts, but that a larger number of impacts on individual boulders may be suitable where boulders are sufficiently large or in short supply (Matthews & Winkler 2022). Given our focus on some of the larger, vegetated moraines from the Early to potentially Middle Holocene (e.g. see Figs 2, 5), large individual boulders were relatively scarce, which necessitated a larger number of impacts on those that were available on each moraine, especially given time constraints at remote field-sites. Thus, the same operator recorded 10 *R*-values from each boulder, with 10 boulders sampled per moraine. The mean was then calculated from the 100 *R*-values from each moraine, and this value was used as the basis for assigning calibrated ages. We acknowledge that this approach is sub-optimal in that it uses relatively small sample sizes (100 *R*-values) from each moraine and may potentially over-sample non-representative boulders, but we note that the results are remarkably consistent in showing an overall down-valley decrease in *R*-value, with statistical tests revealing significant differences between most moraine pairs, which is consistent with a longer duration of exposure for older moraines (see below).

Impacts were made on horizontal or near-horizontal surfaces and were separated by at least a plunger tip width. Readings were made on dry surfaces, away from the edge of boulders or any visible cracks, and rock surfaces were not abraded by carborundum treatment before measurements (e.g. Day 1977; Shakesby *et al.* 2006; Wilson *et al.* 2019). Care was taken to avoid inhomogeneity from structural features such as cleavage/foliation (Matthews & Winkler 2022). Most sampled boulders within Strupskardet and Rotsunddalen were above the treeline. In the few cases where moraines were below the treeline, we avoided boulders directly beneath trees, as these were often covered by grasses, moss, and foliose lichen.

An important limitation of our Schmidt hammer dating was that the lithology of the moraine boulders was different between Rotsunddalen (schist) and Strupskardet (gabbro). Matthews and Winkler (2022) note that it is important to restrict sampling to particular lithologies because weathering rates are likely to differ between rock types. They also acknowledge, however, that in most regional studies that cover multiple locations, this constitutes an ideal that is rarely realized in nature and that lithological compatibility is more realistic and attainable. Given that the moraines in Strupskardet are the only moraines in the study area that have been

Fig. 2. Examples of samples collected for terrestrial cosmogenic nuclide (TCN) dating. A. Oblique view of moraine SM3 (see Fig. 4B) showing the moraine crest (dashed white line) and approximate location of samples (red circles). B. Aerial orthophotograph showing the approximate locations of samples (2016 imagery; www.norgeibilder.no). The images around the sides (panels C–F) show the individual sampled boulders with photographs taken from multiple angles and a blue arrow showing the sampling point. Note: tape extended to 50 cm in each image.

independently dated, we deemed it worthwhile to at least compare Schmidt hammer data from those moraines with those in Rotsunddalen, noting that both gabbro and schist have been classified as 'strong' in studies of the influence of lithology on *R*-values (e.g. Placek & Mignon 2007). We also acknowledge the warning of McCarroll (1989) that although Schmidt hammer data hold potential for measuring rock weathering and interpreting relative age, they should be viewed as a rapid, inexpensive and convenient technique for preliminary assessment. Thus, we view our age calibration using Schmidt hammer data as necessarily preliminary and simply use it alongside other methods to compare with previous chronologies and to develop hypotheses that future work could test.

Soil chronosequencing. – Three or more soil pits were excavated into the crests of moraines that pre-date the LIA maxima (i.e. moraines down-valley from the LIA limits identified in Leigh *et al.* 2020). In Rotsunddalen, 30 soil pits were excavated until the C-horizon was reached. The geomorphological context and vegetation coverage of each moraine/soil pit location were recorded alongside details of crest elevation, approximate height from the valley floor and locality with respect to running and/or standing water. Where possible, pits were constrained to sharp-crested portions of moraines (cf. McCarroll & Ware 1989; Evans 1999). Both lateral and end moraines were sampled, and pits were excavated in areas where surface boulders were fewest, in the hope of encountering fewer obstacles with depth.

Soil horizons were identified based on distinct colour changes (see Birkeland 1999 for rationale and application to Quaternary soils). From the middle of each identified horizon (and the top of the C-horizon) ~100 g of soil was collected for laboratory analysis of dry and wet colour, soil pH, and loss on ignition (LOI) analysis. In each pit, the depth of soil to the base of the B-horizon (top of the C-horizon) and the thickness of each identified horizon (excluding C-horizon) were measured (cf. Evans 1999).

In the laboratory, the colours of the wet and dry soil samples were determined using a Munsell soil colour

chart. Soil colour enrichment of each horizon was then calculated following the colour development equivalent (CDE) of Buntley & Westin (1965), whereby the chroma is multiplied by a soil colour value (e.g. $10R = 7$; $2.5YR = 6$; $5YR = 5$; $7.5YR = 4$; $10YR = 3$; $2.5Y = 2$ and $5Y = 1$). This provided a metric for soil reddening and thus an indication of the maturity of soil development. Soil pH was measured from a 1:2.5 suspension (10 g of dry soil:25 mL of distilled water). Loss on ignition was used to provide an indication of total organic matter content. Around 5 g of each sample was dried overnight at 105 °C to determine moisture content, and the samples were then ignited at 550 °C for 4 h in a furnace to determine percentage LOI.

TCN dating. – Perched boulders and moraine boulders were sampled for cosmogenic ^{10}Be TCN dating to determine the timing of glacier thinning and retreat (Table 1, Fig. 2). In total, 13 samples were collected in August–September 2019. Three perched boulders were sampled at the edge of a bedrock lip approximately halfway up Rotsunddalen, above the moraine on the valley floor, and 10 moraine boulders were sampled, with eight located on the moraine crests and two located on the distal slopes (Fig. 4B).

Sampled surfaces were between 50 and 310 cm from the ground (Table 1) and all samples were removed from the highest point of the host boulder to maximize exposure to cosmic rays and minimize snow cover of the surface. To minimize the likelihood of sampling moraine boulders affected by postdepositional boulder rotation or moraine (de-)stabilization (e.g. melt out of buried ice), we targeted boulders that were partially embedded in the moraine matrix and away from obvious breaches (e.g. caused by postdepositional reworking from meltwater streams). Two samples were found fragmented *in situ* and the remainder were collected using hammer and chisel; an average sample thickness was calculated from multiple measurements of every sample fragment. Azimuthal elevations were measured in the field using a standard geological compass and clinometer. Sample locations and elevations were recorded using a Garmin GPSMAP® 64 s with GLONASS (±3 m).

Sample processing and measurement were carried out at the Cosmogenic Isotope Analysis Facility, Scottish Universities Environmental Research Centre (CIAF–SUERC), following the procedures of Mendelová *et al.* (2020). The ^{10}Be concentrations are based on the 2.79×10^{-11} ^{10}Be/^{9}Be ratio for NIST SRM4325. The processed blank ratio was between 3 and 10% of the sampled ^{10}Be/^{9}Be ratios and was subtracted from the sample ratios. The uncertainty of this correction is included in the stated standard uncertainties. The ^{10}Be/^{9}Be ratios were measured and calculated on the 5 MV accelerator mass spectrometer at SUERC.

The TCN surface-exposure ages were calculated using the Cosmic Ray Exposure program (Martin *et al.* 2017). We applied a local production rate (weighted mean of 3.40±0.24 atoms g^{-1} a^{-1}; sea level high latitude) based on two calibration sites in Arctic Norway (the Grotlandsura and Russenes rock avalanches; see Fenton *et al.* 2011), and also separately applied a global production rate (weighted mean of 3.98±0.22 atoms g^{-1} a^{-1}; sea level high latitude) for comparison purposes. The age calculations additionally used the time-dependent LSD scaling scheme with ERA40 atmosphere model (Lifton *et al.* 2014).

We also applied a number of corrections to account for the potential effects of surface erosion, snow cover and glacial isostatic adjustment using the iceTEA tool (Jones *et al.* 2019a). Subaerial erosion of a boulder surface can occur following its exposure, resulting in a loss of nuclides. To minimize this impact, we sampled boulder surfaces with the least amount of postdepositional surface erosion. However, samples may plausibly have lost ~1 to 10 mm from the surface and so we applied a potential surface erosion correction of 10 mm ka^{-1}, calculated using the iceTEA tool with the global production rate. Snow cover can influence the production rate through partial shielding of the boulder surface from cosmic rays. The amount of snow that can limit nuclide production depends on the density of the snow and, crucially, the thickness and duration of that snow cover, which is extremely challenging to constrain in the past (Ye *et al.* 2023). To minimize the influence of snow cover, we sampled top surfaces of large boulders, which would most likely be above-ground snow and be more easily windswept, but snow cover cannot be ruled out and so we used iceTEA to estimate the impact of snow cover providing 20% shielding, using the global production rate. Finally, glacial isostatic adjustment can influence the production rate at a given site. The production rate is dependent on elevation, which changes over time owing to glacial isostatic adjustment, potentially causing TCN ages to overestimate or underestimate the true exposure time (Jones *et al.* 2019b). Isostatic uplift owing to the deglaciation of the Fennoscandian Ice Sheet means that the production rate was probably lower at the time of exposure (lower elevation relative to today) and so we applied a correction to account for this using iceTEA with the ICE-6G model and global production rate.

Results

Central Troms and Finnmark moraine distribution and morphology: regional context

Here, we briefly describe and illustrate some of the key features in the glacial geomorphological map from Leigh *et al.* (2021) that underpins our palaeoglaciological reconstruction and provides a regional context for our more detailed field observations that follow. It is clear that the glacial geomorphology in central Troms and

Table 1. Details for terrestrial cosmogenic nuclide (TCN) samples collected from Sorbmevággi and the main part of Rotsunddalen.

Feature	Sample ID	Latitude (decimal degrees)	Longitude (decimal degrees)	Elevation (m a.s.l.)	Sample location	Boulder size (cm) ($L \times W \times H$)	Surface height from ground (cm)	Lithology	Sample thickness (cm)	Density (g cm^{-3})	Shielding factor
Knoll	RV-19-18B	69.72371	20.70187	387	Bedrock lip[1]	110 × 100 × 60	60	Quartz vein in schist	0.7	2.7	0.990345
Knoll	RV-19-20B	69.72525	20.69647	367	Bedrock lip[1]	110 × 80 × 90	90	Quartz vein in schist	0.8	2.7	0.984009
Knoll	RV-19-21B	69.72483	20.69754	390	Bedrock lip[1]	65 × 50 × 50	50	Quartz vein in schist	3.9	2.7	0.983618
SM1	RV-19-15 M	69.72691	20.70633	205	Moraine crest[2]	300 × 260 × 90	90	Schist	1.7	2.7	0.982982
SM1	RV-19-17 M	69.72680	20.70222	256	Moraine crest[2]	250 × 140 × 110	110	Schist	1.3	2.7	0.983949
SM3	RV-19-09 M	69.72878	20.69175	264	Top of distal slope[2]	250 × 330 × 310	310	Schist	1.4	2.7	0.959812
SM3	RV-19-10 M	69.72864	20.69175	280	Moraine crest[2]	150 × 80 × 85	85	Quartz vein in schist	1.8	2.7	0.967002
SM3	RV-19-11 M	69.72665	20.69271	279	Top of distal slope[2]	350 × 150 × 175	175	Schist	4.0	2.7	0.962396
SM3	RV-19-16 M	69.72698	20.69328	269	Moraine crest[2]	330 × 110 × 75	75	Schist	1.5	2.7	0.972585
SM4	RV-19-05 M	69.72533	20.68416	279	Moraine crest[2]	160 × 100 × 65	60	Gneiss	3.5	2.7	0.966573
SM4	RV-19-07 M	69.72604	20.68044	284	Moraine crest[2]	110 × 80 × 55	55	Gneiss	3.0	2.7	0.958737
SM5	RV-19-01 M	69.72257	20.67165	312	Moraine crest[2]	220 × 115 × 90	60	Schist	5.0	2.7	0.951616
SM5	RV-19-04 M	69.72345	20.67528	302	Moraine crest[2]	210 × 190 × 170	180	Quartz vein in schist	0.6	2.7	0.959006

[1]Samples collected above the moraines, within the main part of Rotsunddalen.
[2]Samples collected from within Sorbmevággi.

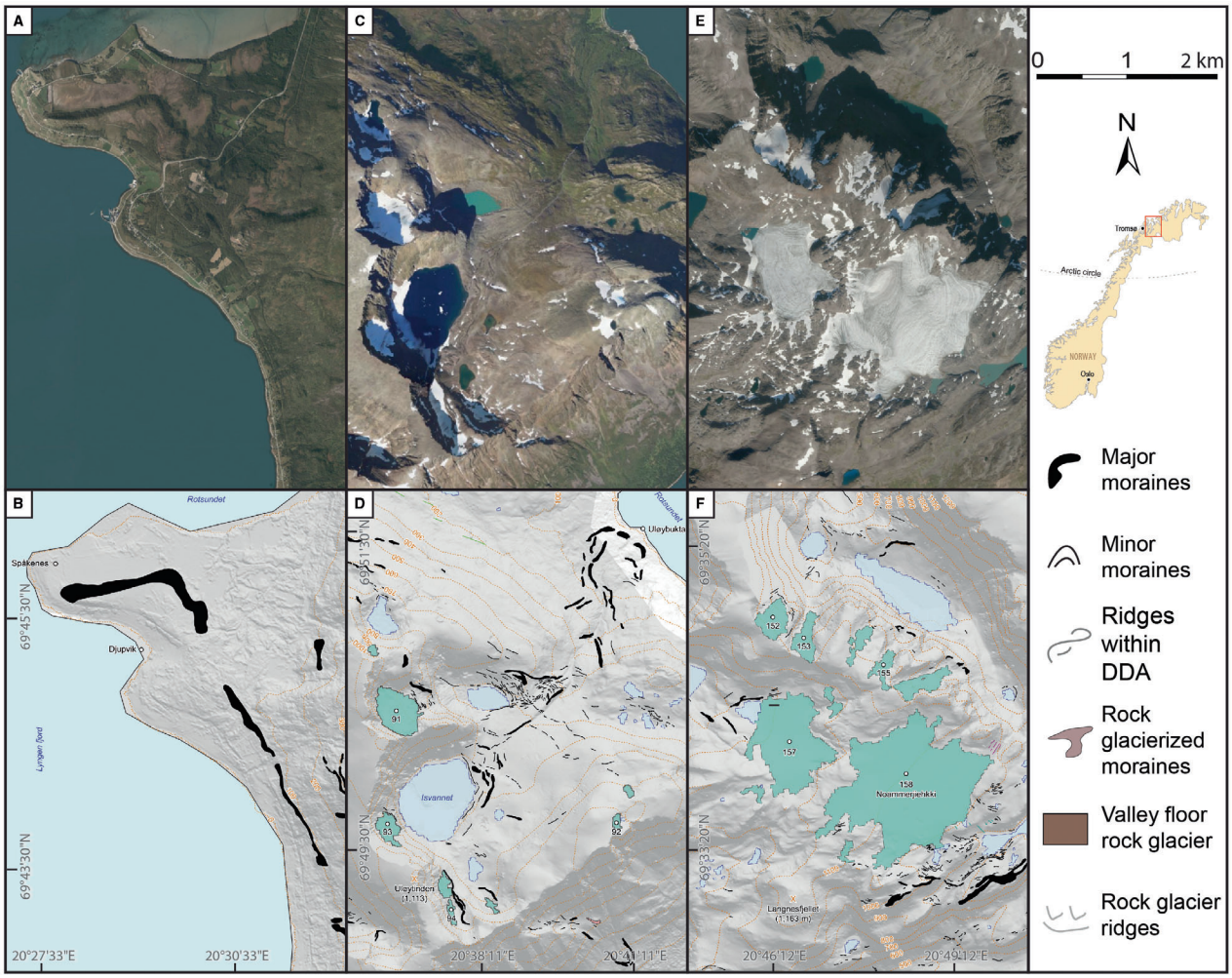

Fig. 3. Excerpts from the mapping of Leigh *et al.* (2021) showing: (A, B) the Spåkenes moraine, part of the Tromsø–Lyngen moraine complex found at the head of Lyngen fjord; (C, D) the large valley moraine system on the island of Ulløya, with latero-frontal moraine extending to near sea level; (E, F) the disintegrating Noammerjiehkki plateau ice cap and surrounding glaciers in the Kåfjord mountains; (G, H) a series of inset arcuate moraines large moraines NW of Lake Guolasjávri; (I, J) closely spaced arcuate moraines on the upland plateau; (K, L) well-defined moraines in Strupskardet appearing largely equally spaced in an up-valley direction. Imagery in the top panels (A, C, E, G, I, K) was captured on 24 August 2016 and is from www.norgeibilder.no. Maps in the bottom panels (B, D, F, H, J, L) are excerpts of the map published in Leigh *et al.* (2021), with a hill-shaded Arctic DEM for background (courtesy of the Polar Geospatial Centre).

Finnmark reflects the combined effects of the retreat of the main Fennoscandian Ice Sheet and its fragmentation into plateau icefield, valley and cirque glacial systems. The largest moraine complexes across the region are those traceable across several large fjords and valley systems, known as the Tromsø–Lyngen moraines (Marthinussen 1962; Holmes & Andersen 1964; Andersen 1968; Vorren & Plassen 2002) and thought to have formed during the early to mid-YD (Jansen *et al.* 2023). The Tromsø–Lyngen moraines can be traced nearly continuously across the study area and frontal portions are clearly identifiable at the fjord heads (cf. Leigh *et al.* 2021). Within the study area, the most clearly identifiable portion of the Tromsø–Lyngen moraine complex is the Spåkenes moraine (Marthinussen 1962), found at the head of Lyngen Fjord (Fig. 3A, B). Additional large moraine complexes are found in the south/SE of the region, across the upland plateau (Fig. 2G, J). Age constraints for these moraines are lacking but it is likely, based upon the close spacing of several arcuate moraine sequences, that these moraines represent short-term fluctuations/stabilizations during overall retreat of the ice margin (e.g. Fig. 3G, H).

The north-eastern side of the Lyngen Peninsula and the coastal islands of Kågen and Ulløya (Fig. 1) are outside the limits of the Tromsø–Lyngen moraines and were likely to have been isolated from the Fennoscandian Ice Sheet during the YD/Tromsø–Lyngen event (Kverndal & Sollid 1993; Evans *et al.* 2002; Hughes *et al.* 2016). At these sites, the glaciated valley landsystem dominates

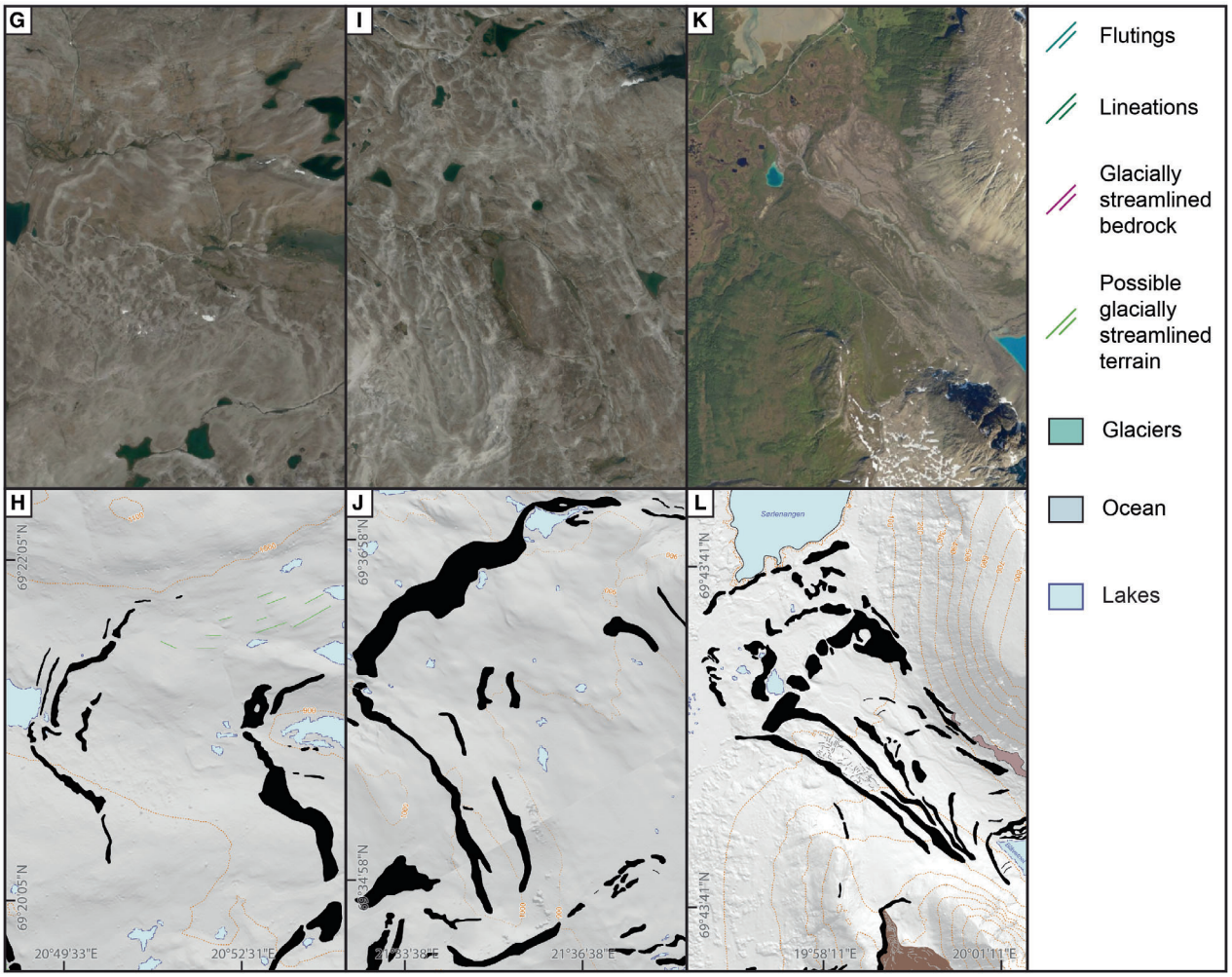

Fig. 3. (Continued)

(Fig. 3C, D). There is also evidence of periglacial activity following deglaciation, characterized by the development of several large rock glacier complexes that are mapped (cf. Leigh *et al*. 2021; Rouyet *et al*. 2021). The NW-orientated valleys of northern Lyngen and the NE-orientated Kågen and Ulløya valleys have some of the most extensive, numerous and distinctive inset sequences of moraines throughout the region (e.g. Fig. 3C, D). Bracketing ages on a select few moraines indicate that some may have been formed prior to the YD, e.g. in Strupskardet (Bakke *et al*. 2005b).

A diverse suite of glacial geomorphological features has been mapped in the mountains of southern Lyngen, north and south of Kåfjord, the Kvænangstinden massif (after the tallest mountain Store Kvænangstinden: 1178 m a.s.l.), as well as across the Riehppe plateau (cf. Leigh *et al*. 2021). Most notable are the smaller, but well-defined moraine sequences located just beyond the valley mouths and inset up-valley (e.g. Fig. 3K, L) and proximal to present-day glacier margins, or empty cirques. There are also sporadic moraine deposits radiating around the mountain plateaus; these fragmentary deposits probably record the presence of old plateau icefields emerging from the flat-topped summits (e.g. Rea & Evans 2007). On the isolated plateaus throughout the study area, the present-day glaciers that remain (e.g. glaciers 157 and 158 (Noammerjiehkki) in the Kåfjord mountains) are currently in a phase of rapid retreat (Leigh *et al*. 2020). These glaciers retain the form of small mountain icefields, with short ice tongues (less than a few hundred metres) filling topographic depressions (Fig. 3E, F). A substantial proportion of rock glaciers are also found within these valley systems (Rouyet *et al*. 2021).

Rotsunddalen moraine morphology

Hjemtverrdalen. – In Hjemtverrdalen (forelands of glaciers 115 and 117; Figs 1Bi, 4A) a series of three near-continuous latero-frontal moraines were studied. The oldest frontal moraine (HM1; Fig. 4A) extends

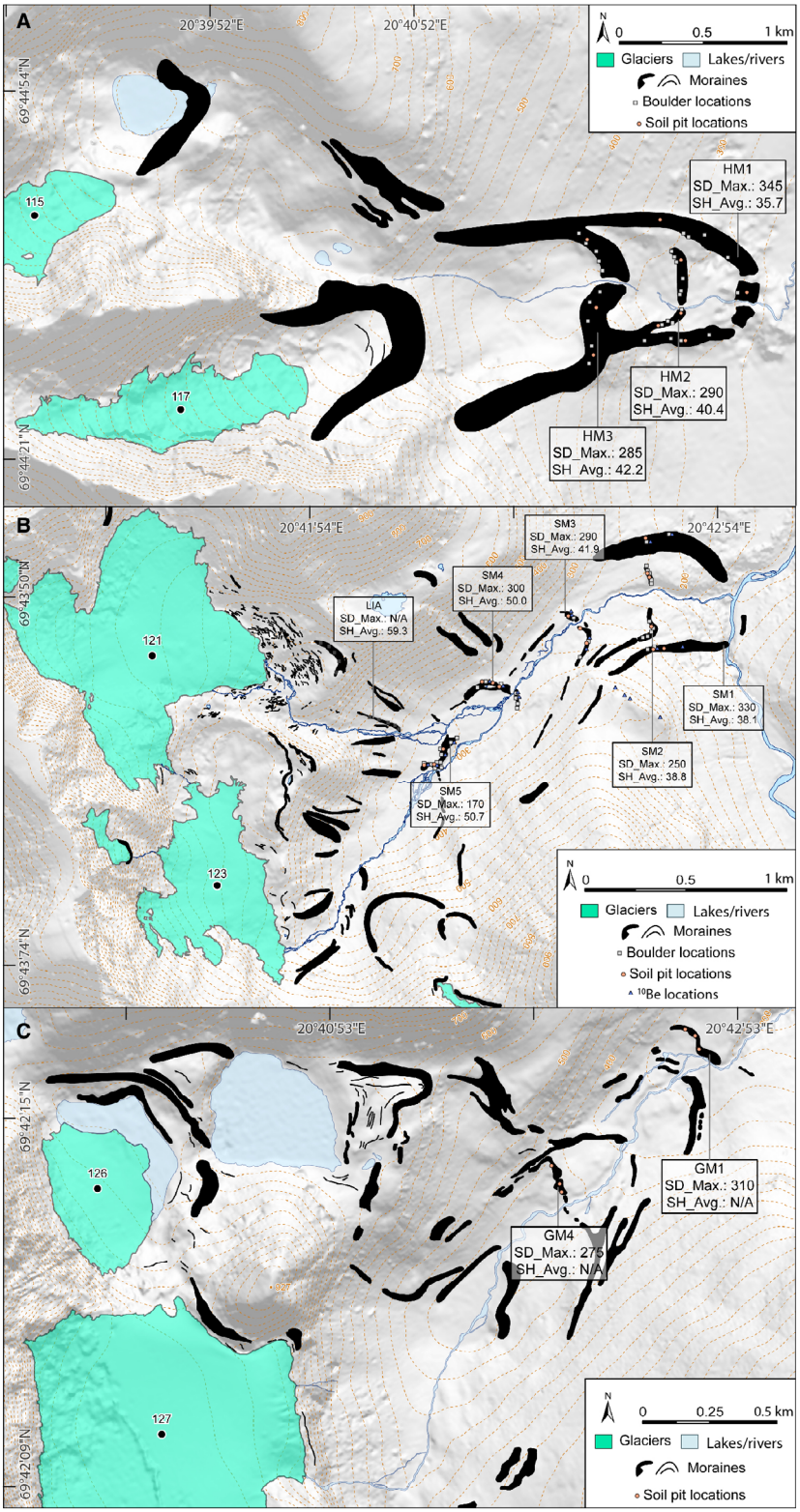

Fig. 4. Moraine mapping of the three subsidiary valleys that feed into Rotsunddalen. A. Hjemtverrdalen. B. Sorbmejiehkki. C. Goahtevággi. All sampled moraines are labelled with their associated maximum soil depth (depth to top of C-horizon; SD_Max) and average Schmidt hammer *R*-value (SH_Avg). Base image is the Arctic DEM (courtesy of the Polar Geospatial Centre).

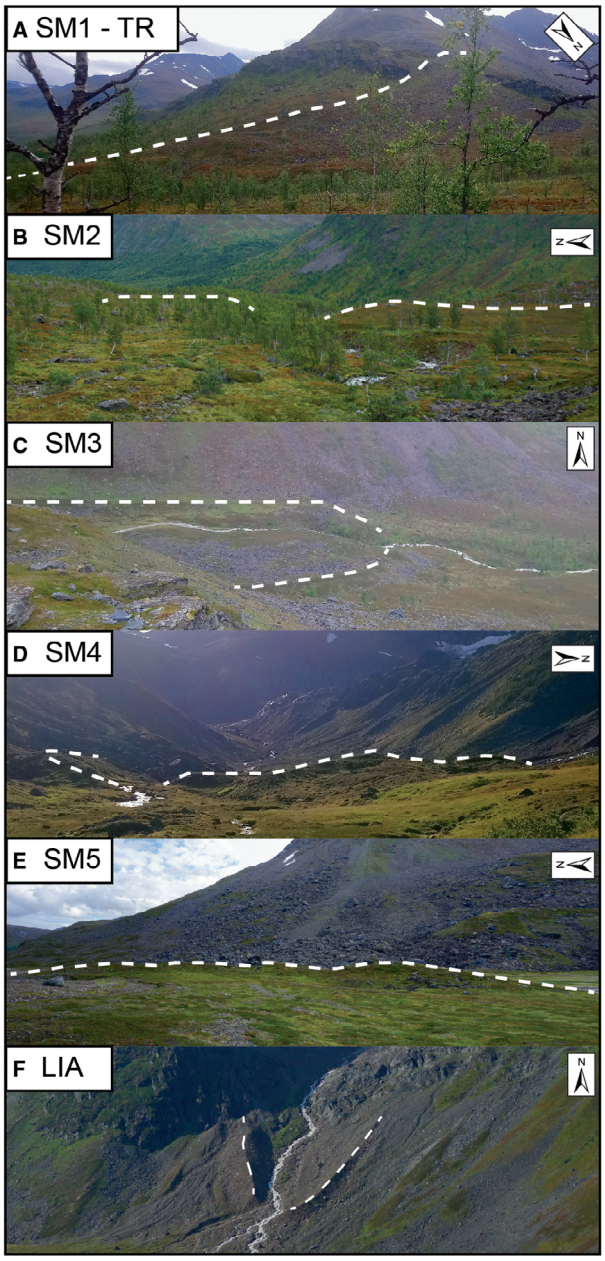

Fig. 5. Photographs showing the Sorbmejiehkki moraine succession from the largest identifiable terminal moraine (SM1) to the LIA moraine (Leigh *et al.* 2020). The white dashed line represents the moraine crest (see Fig. 4 for geomorphological map).

~1 km into the main part of Rotsunddalen and has a steep, 20-m-high distal slope and shallow proximal slope both rising to a well-defined crest up to ~5 m wide. Inside HM1 and located ~160 m up-valley is a smaller frontal moraine, HM2 (Fig. 4A), which is characterized by a ~7-m-high distal slope and a broad crest. The youngest moraine examined (HM3; Fig. 4A) is located ~190 m up-valley from HM2 and is characterized by a very steep and ~30 m-high distal slope with broad crested (~5-m wide) lateral ridges and narrower (2–3 m wide) frontal ridge.

Sorbmevággi. – Sorbmevággi (foreland of glaciers 121 and 123; Figs 1Bii, 4B) contains a complex succession of moraines, five of which were studied in detail. The oldest moraine (SM1; Figs 4B, 5A) extends ~0.8 km out of Sorbmevággi into the main part of Rotsunddalen (between 2.6 and 2.9 km from the present-day glaciers 121 and 123, respectively). In its lateral portions, it has a steep distal slope with a height of ~10 m, rising to a well-defined crest on the true right (up to ~5 m wide), while on the true left, the crest is poorly defined with multiple ridge features recording either moraine de-stabilization (e.g. melt of buried ice core) or postdepositional reworking (e.g. input from rock-avalanche deposits). The proximal slope is steep and ~10-m high, and, on the true right, has smaller ridges inset against it.

Inside the SM1 lateral moraine is a small, recessional moraine (SM2; Figs 4B, 5B), which is the most subdued moraine in the succession with a near symmetrical proximal and distal slope. It rises to a height of ~7 m on the true right but only ~2 m on the true left. SM2 is positioned at the edge of the treeline with well-established birch trees having colonized its slopes.

Located ~400 m up valley and at the head of Sorbmevággi is an imposing latero-frontal moraine (SM3; Figs 4B, 5C), which extends across the whole valley floor. Its frontal portion has a steep distal slope more than 10-m high, a well-defined crest ~2 to 3-m wide, and a steep proximal slope (~5-m high), best preserved on the true left. On the true right, a series of complex ridges within DDAs occur on the proximal slopes of SM3. The DDAs are small areas of complex, hummocky, terrain manifest as a disorganized ridge and furrow network separated by a mix of sediment veneer, rocky and bouldery debris, and vegetated ground (Leigh *et al.* 2021). The lateral portion of SM3 lies low on the valley sides. On the true left it extends only part way into Sorbmevággi where it is overridden by colluvium; on the true right it can be traced for an additional ~340 m before it becomes indistinguishable from the area of DDA.

Located ~450 m up valley from SM3 is another latero-frontal moraine (SM4; Figs 4B, 5D) with steep distal and proximal slopes <10-m high and a broad crest, which in some places is poorly defined. The lateral portions are clearly defined on both sides of the valley for ~130 m, after which colluvium on the true left overrides the feature and DDA is developed on the true right.

Inside SM4, on the true right side of Sorbmevággi and located ~350 m up valley, and ~250 m outside the LIA moraine, is a fragmented latero-frontal moraine (SM5; Figs 4B, 5E). The distal slope is steep and ranges from ~5 to ~15 m high. The crest is well defined (2–3-m wide), and the proximal slope is short and shallow. SM5 has been fragmented, presumably by postdepositional meltwater drainage, and is identifiable as a ~160-m-long frontal

Table 2. Schmidt hammer *R*-values from moraines within Strupskardet and Rotsunddalen. Note that no Schmidt hammer readings were taken from Goahtevággi.

Site	Moraine age[1] (ka) or moraine ID	Moraine mean *R*-value±95% CI	Feature skewness	Feature kurtosis
Strupskardet	9.3–8.9 (M12)[1]	41.2±1.2	0.06	−0.20
	9.8–9.4 (M11)[1]	38.1±2.3	0.48	0.74
	12.0–11.6 (M9)[1]	36.0±1.5	0.33	−0.04
	12.6–12.4 (M8)[1]	36.4±1.2	0.05	−1.09
Sorbmevággi	SM LIA	59.3±1.2	−0.89	0.86
	SM5	50.7±1.5	−0.37	0.26
	SM4	50.0±1.2	−0.78	0.63
	SM3	41.9±1.3	−0.19	−0.27
	SM2	38.8±1.7	−0.05	−0.52
	SM1	38.1±1.6	−0.06	−0.51
Hjemtverrdalen	HM3	42.2±1.3	−0.56	0.56
	HM2	40.4±2.8	−0.27	−0.54
	HM1	35.7±1.6	0.04	−0.22

[1]Bracketing moraine ages and moraine IDs from Bakke *et al.* (2005b).

portion and a 180-m-long lateral portion that grades up to the valley side bedrock face. In the frontal portion of SM5, the distal slope is partly superimposed by an area of rock slope failure deposits, clearly distinguishable from the glacial deposits by their size, angularity and positioning within the valley. On the true right, SM5 shows signs of bifurcation where two ridges emerge from one in its central portion. This may have been caused by melt out of buried glacial ice or by a dynamic frontal margin.

Goahtevággi. – In Goahtevággi (foreland of glaciers 126, 127, 129, 131 and 132; Figs 1Biii, 4C) only two moraines were studied. These moraines are heavily vegetated and do not contain large, exposed boulders on their crest and, therefore, it was not possible to collect Schmidt hammer rebound values. Unlike in Hjemtverrdalen and Sorbmevággi, the oldest moraine (GM1; Fig. 4C) does not extend into the main part of Rotsunddalen, but is instead situated at the head of Goahtevággi and only accessible on its true left. GM1 is a low-lying, broad feature situated on a wide, flat surface ~130 m higher than the main part of Rotsunddalen floor. The moraine has a steeper and higher proximal slope than distal slope and cannot be traced along the valley sides. Overall, GM1 is the most fragmented and subdued feature studied, probably resulting from postdepositional re-working.

Around 700 m up valley from GM1 is a much larger latero-frontal moraine that spans the full width of Goahtevággi (GM4; Fig. 4C) and is ~1.2 km from glacier 127. There are two additional moraines between this moraine (GM4) and the outermost moraine (GM1), but GM4 was selected for sampling as it was interpreted to be the last moraine that was formed when the glaciers at the head of this catchment were confluent and should therefore provide an indication of glacier activity midway through the moraine sequence. GM4 can be traced along the valley walls and is only breached by the Goahtejohka river channel. Its distal slope is steep and ~30-m high and it has a broad crest (~15-m wide) and a shallower proximal slope that is overlain/overlapped by multiple ridges and ridge-like features (DDAs).

Schmidt hammer data

A total of 110 boulders were sampled from moraines in Strupskardet and Rotsunddalen, with a total of 1100 readings (*R*-values). The range in mean *R*-values across our entire dataset is broad, extending from 59 on the Sorbmevággi LIA moraine (SM LIA; Table 1) to 35 on the Hjemtverrdalen terminal moraine (HM1; Table 2). While there is a high variability in the *R*-values on individual boulders (see Figs S1, S2) and despite our sub-optimal sampling strategy (see above), there is an overall down-valley decrease in *R*-values, consistent with results from other investigations that have used the Schmidt

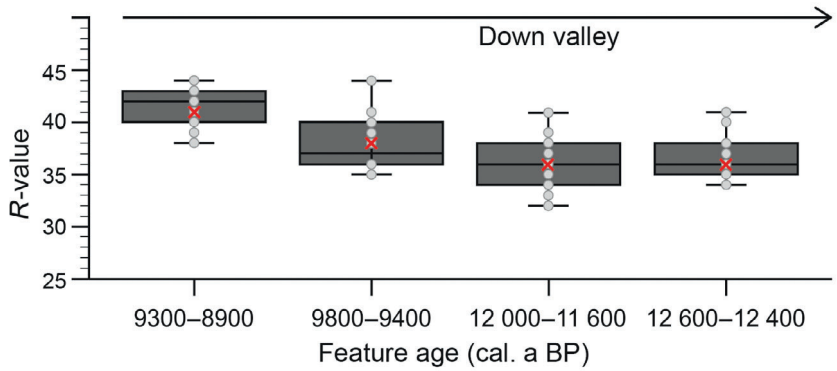

Fig. 6. Box plots of Schmidt hammer *R*-values from Strupskardet moraines with independent age control from Bakke *et al.* (2005b). Light grey dots represent the mean *R*-values from individual boulders (see also Fig. S1), while the red crosses represent the mean *R*-value for each moraine. The dark grey box shows the interquartile range, the black horizontal line the median and whiskers show the minimum and maximum *R*-values for each moraine.

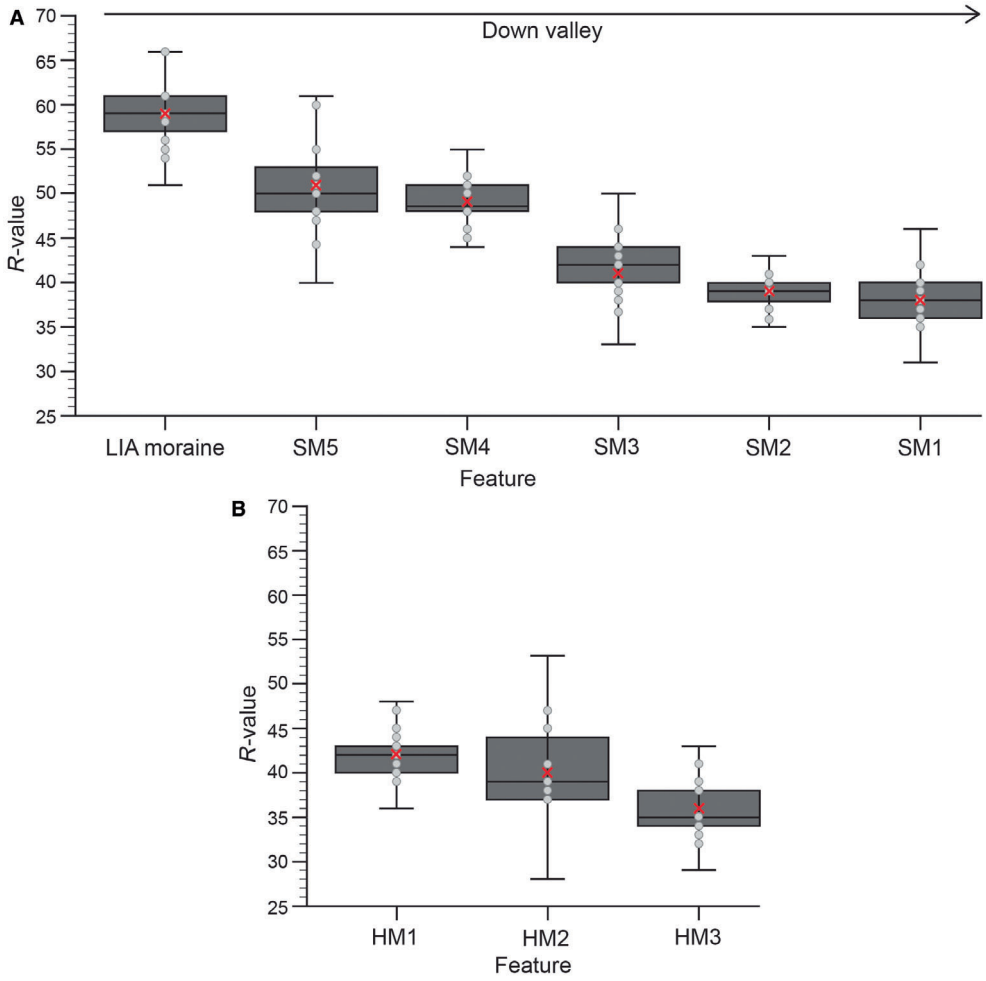

Fig. 7. Box plots of Schmidt hammer *R*-values from: (A) Sorbmevággi moraines and (B) Hjemtverrdalen moraines. Light grey dots represent the mean *R*-values from individual boulders (see also Fig. S2), while the red crosses represent the mean *R*-value for each moraine. The dark grey box shows the interquartile range, the black horizontal line the median and whiskers show the minimum and maximum *R*-values for each moraine.

hammer to establish moraine ages in Norway and elsewhere (e.g. Matthews & Winkler 2011; Winkler 2014; Tomkins *et al*. 2018).

Strupskardet. – The *R*-values from the moraines of Strupskardet (Table 2, Fig. 6) show a clear decrease with distance down-valley (i.e. moraine relative age). Use of a two-sample *t*-test indicates that mean *R*-values from most moraines represent significantly different populations (p-values <0.05), apart from the M8 (12.8–12.4 ka) and M9 (12.0–11.6 ka) moraines, which have p-values >0.05 (0.67), which is to be expected given their similar age in Bakke *et al*. (2005b) (Table 2).

Rotsunddalen. – Schmidt hammer measurements were only possible within Hjemtverrdalen and Sorbmevággi and not in Goahtevággi. The most extensive Schmidt hammer dataset was established in Sorbmevággi and *R*-values there show a clear decrease with distance down-valley (Table 2, Figs 4B, 7A). Use of a two-sample *t*-test confirms that mean *R*-values from four of the six moraines represent significantly different populations ($p < 0.05$). Moraines SM5 and SM4, alongside SM2 and SM1, however, have p-values >0.05.

The *R*-values from the moraines of Hjemtverrdalen (Table 2, Figs 4C, 7B) suggest two sets of moraines that show a reduction in *R*-value with distance down-valley (i.e. moraine relative age). Use of a two-sample *t*-test indicates that HM3 and HM2 do not represent significantly different populations, but HM3/HM2 and HM1 represent significantly different populations.

Soil chronosequences

For most soil pits excavated in Rotsunddalen, the surface vegetation consisted of a dispersed to thick matt of plants from the *Vaccinium* and *Empetrum* genus of dwarf shrubs (e.g. bilberry and/or crowberry) and/or a variety of mosses and lichens such as juniper haircap moss (*Polytrichum juniperinum*) and reindeer lichen (*Cladonia*

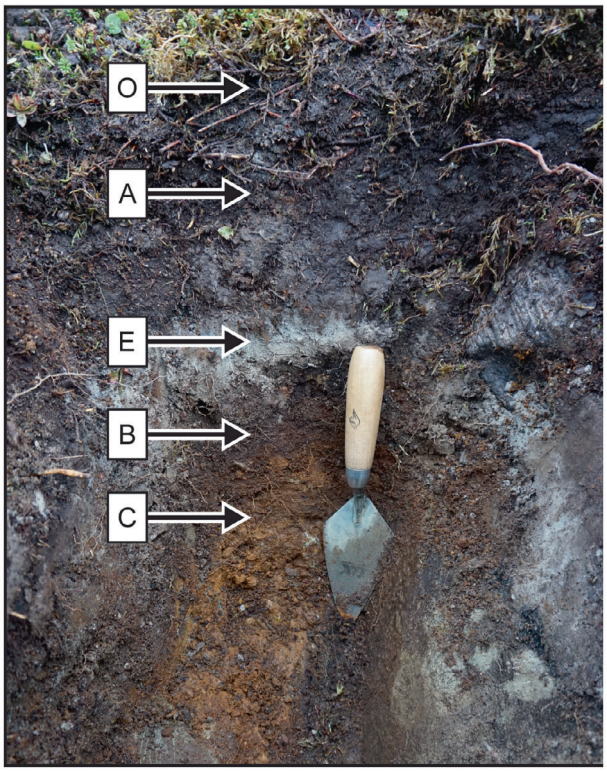

Fig. 8. Soil profile found in Rotsunddalen (pit RV-19-SP22) from the moraine crest, with major soil horizons labelled (see text for explanation). Trowel is 127 mm long.

rangiferina). Additionally, some soil pits were within the treeline of well-established downy birch (*Betula pubescens*). Owing to the mountainous terrain and isolation of the sites, it is assumed that no major anthropogenic land management has occurred since deglaciation. Hence the soils are unaltered and present a natural chronosequence of soil development.

Of the 30 soil pits examined, 29 are classified as Haplic Podzols (Ellis 1979; cf. Bridges 1997) exhibiting a distinct E-horizon of ash-grey colour (Fig. 8), and one pit (RV-19-SP18) was considered a Cambic Podzol (Bridges 1997) on the basis that no distinct grey E-horizon was present. The podsolization of the soils is indicative of the long, cold winters and short mild summers of the region, and the Taiga biome that dominates the forelands at the elevations of the moraines examined (Fitzpatrick 1983; Evans 1999). The examined soils (e.g. Fig. 8) generally comprised a thin layer of organic matter and vegetation on the surface (O-horizon), directly underlain by a very dark (near black) layer of soil (A-horizon), rich in organic material and in many cases held together by a thick matt of roots. Below the A-horizon is the characteristic eluvial E-horizon, forming a striking 'ash-grey' layer from which minerals have been leached. Beneath the E-horizon is the illuvial B-horizon, comprising parent material which has been altered by pedogenic processes and in which minerals accumulate, having been leached from the E-horizon above. The B-horizon is firmer in texture than the horizons above, with a darker brown colour and often intermixed with larger clasts. Finally, the B-horizon transitions sharply into a compact C-horizon of unaltered parent material, often with closely packed, larger clasts. The C-horizon is also recognisable by its lighter colour than the soil above, its coarser texture and the lack of visible organic material (e.g. roots). In one instance (RV-19-SP08), a layer of reddened material was found between the B and C-horizon, interpreted as a layer of oxidized parent material and denoted as a Cox-horizon (oxidized C horizon; Birkeland 1978).

Rotsunddalen. – Of the three subsidiary valleys within Rotsunddalen (Hjemtverrdalen, Sorbmevággi, and Goahtevággi; Fig. 1B), the most extensive chronosequence was established in Sorbmevággi (Fig. 4B). Thus, the Sorbmevággi chronosequence was used as a baseline from which comparisons of soil development within Hjemtverrdalen and Goahtevággi are made. The general soil profiles in Sorbmevággi (Fig. 9) reveal that, although there is some intra-landform variation between soil pits, the overall trend is one of increasing soil depth with distance down-valley (i.e. with their inferred relative age; SM5-SM1). For example, the youngest pre-LIA moraine (SM5) has a maximum soil depth to the base of the B-/top of C-horizon of 170 mm, whereas the oldest moraine (SM1) has a maximum depth of 330 mm (Table 3). There is, however, one notable outlier in this trend; the small end moraine (SM2) has considerably thinner and shallower soils than expected based upon its position within the moraine succession.

The specific B-horizon characteristics from each soil pit in Sorbmevággi (Table 3) show a mix of changes in the CDE of both wet and dry B-horizons and indicate no strong pattern of increasing soil reddening with increasing distance down-valley (i.e. with increasing moraine relative age), as might have been expected based on previous work with alpine soils in Norway (e.g. Evans 1999). Generally, the pH of the B-horizon is that of decreasing acidity with distance down-valley, with the outermost soils being the most alkaline. Finally, the percentage of organic matter in the B-horizon of each moraine, established via LOI, generally increases

Fig. 9. Soil profiles from each soil pit on the moraines sampled in Sorbmevággi. A. SM5. B. SM4. C. SM3. D. SM2. E. SM1 (see Fig. 4B for location). Showing soil horizons (A- to C-horizon), wet soil colour (using Munsell colour notation), wet soil colour development equivalent (CDE; following Buntley & Westin 1965), loss on ignition (LOI) values and soil pH.

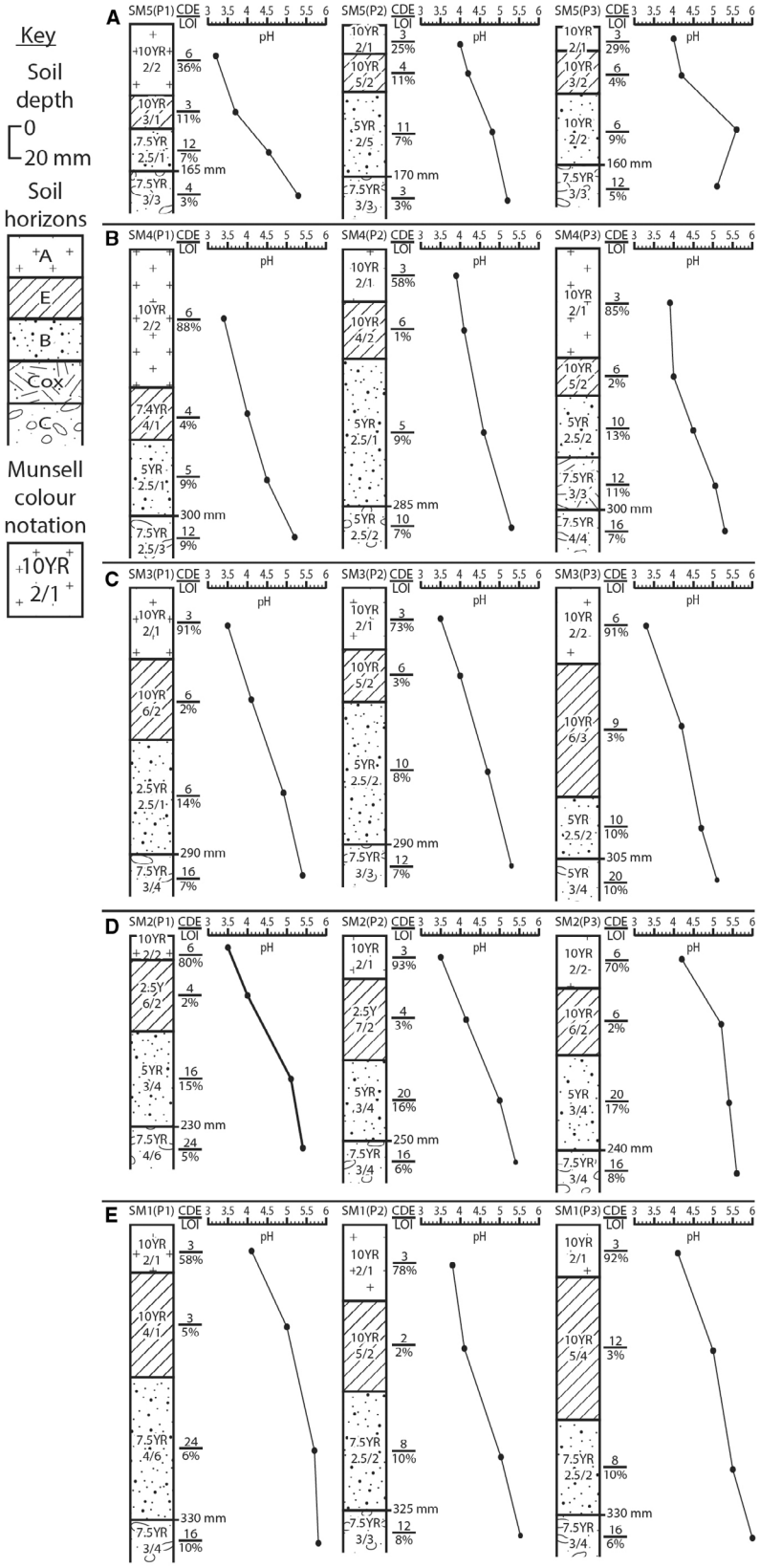

Table 3. Soil characteristics from moraines within Rotsunddalen. Note that some measurements are not available (denoted by a dash) owing to Covid-19 laboratory closures.

Site	Moraine ID	Soil pit ID	Soil sample ID	B-horizon											
				CDE[1]	Mean CDE[1]	CDE[2]	Mean CDE[2]	Organic content (%)	Mean organic content	pH	Mean pH	Thickness (mm)	Mean thickness (mm)	Depth[3] (mm)	Mean depth[3] (mm)
Sorbmevággi	M5	SM5(P1)	RV-19-SP03B	4	6.7	16	16	7		4.5		45		165	
		SM5(P2)	RV-19-SP04B	10		16		11	9	4.8	5.0	90	70	170	165
		SM5(P3)	RV-19-SP05B	6		16		9		5.6		75		160	
	M4	SM4(P1)	RV-19-SP06B	5	6.7	12	11.3	9		4.5		80		300	
		SM4(P2)	RV-19-SP07B	5		10		9	10	4.6	4.5	155	100	285	277
		SM4(P3)	RV-19-SP08B	10		12		13		4.5		65		245	
	M3	SM3(P1)	RV-19-SP09B	6	8.7	24	20	14		4.9		120		290	
		SM3(P2)	RV-19-SP11B	10		12		8	11	4.7	4.8	150	112	290	295
		SM3(P3)	RV-19-SP12B	10		24		10		4.7		65		305	
	M2	SM2(P1)	RV-19-SP01B	20		24		15		5.2		100		230	
		SM2(P2)	RV-19-SP02B	20	20	18	20	16	16	5.0	5.2	85	95	250	240
		SM2(P3)	RV-19-SP15B	20		18		17		5.4		100		240	
	M1	SM1(P1)	RV-19-SP10B	24		18	20	6		5.7		150		330	
		SM1(P2)	RV-19-SP13B	8	13.3	24		10	9	5.1	5.4	125	125	325	328
		SM1(P3)	RV-19-SP14B	8		18		10		5.5		100		330	
Hjemtverrdalen	M3	HM3(P1)	RV-19-SP16B	10	5.7	16	17.3	–		4.9		70		270	
		HM3(P1)	RV-19-SP17B	3		12		–	–	5.1	5.3	80	90	230	262
		HM3(P3)	RV-19-SP18B	4		24		–		5.8		120		285	
	M2	HM2(P1)	RV-19-SP22B	8	8	12	18	–		4.9		55		290	
		HM2(P1)	RV-19-SP23B	8		18		–	–	4.9	5.0	80	63	220	252
		HM2(P3)	RV-19-SP24B	8		24		–		5.1		55		245	
	M1	HM1(P1)	RV-19-SP19B	24	15.3	18	18	–		5.3		145		345	
		HM1(P1)	RV-19-SP20B	10		18		–	–	5.9	5.5	135	130	265	305
		HM1(P3)	RV-19-SP21B	12		18		–		5.4		110		305	
Goahtevággi	M_	GM_(P1)	RV-19-SP28B	4	3.3	12	12	–		5.0		65		225	
		GM_(P2)	RV-19-SP29B	2		16		–	–	5.3	5.4	70	60	240	247
		GM_(P3)	RV-19-SP30B	4		8		–		5.8		45		275	
	M1	GM1(P1)	RV-19-SP25B	10	9.3	18	18	–		4.9		85		290	
		GM1(P2)	RV-19-SP26B	10		18		–	–	5.4	5.2	110	105	310	297
		GM1(P3)	RV-19-SP27B	8		18		–		5.4		120		290	

[1]Colour development equivalent (CDE) of wet soil (Buntley & Westin 1965).
[2]CDE of dry soil (Buntley & Westin 1965).
[3]Depth to base of B-horizon/top of C-horizon.

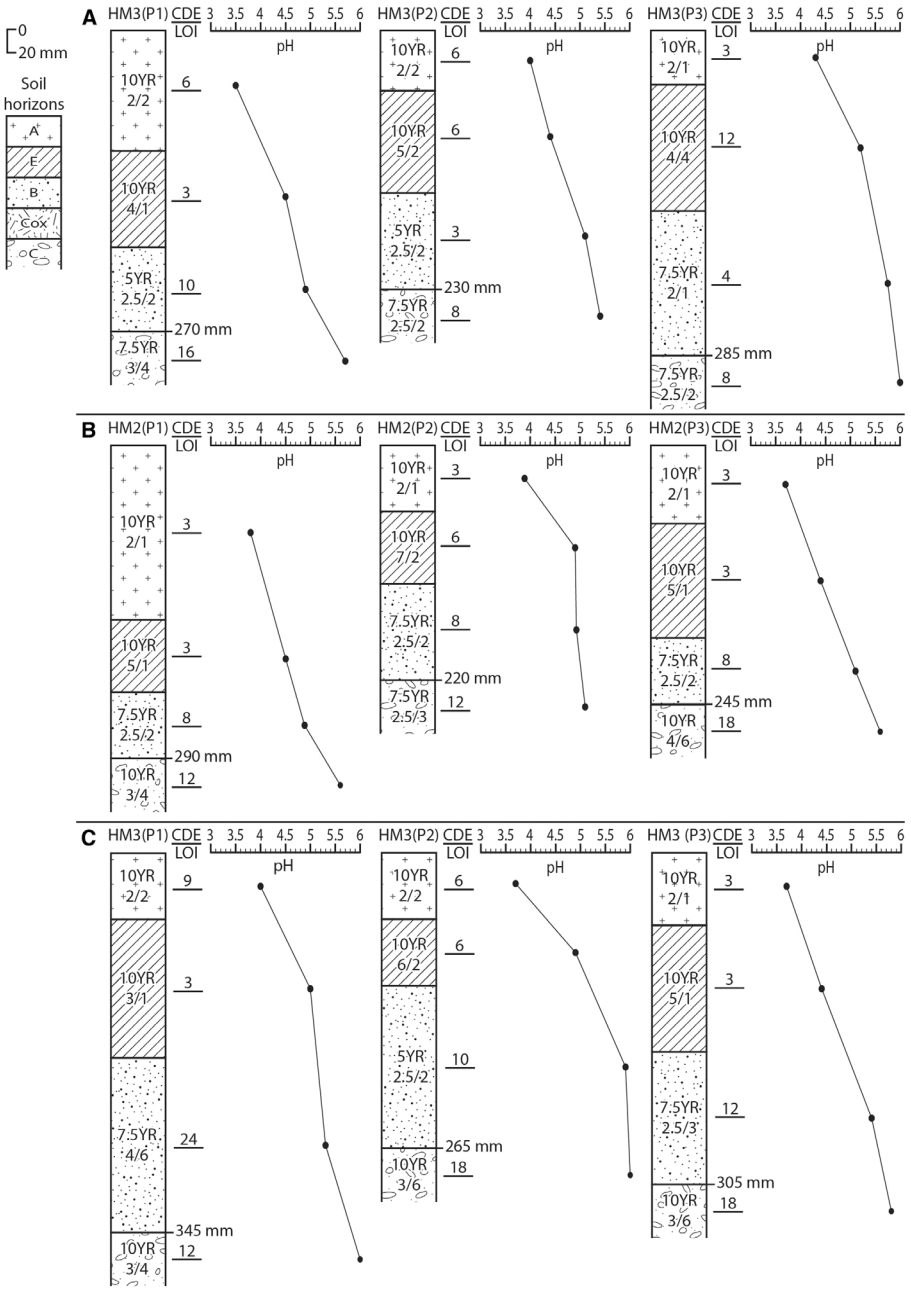

Fig. 10. Soil profiles from each soil pit on the moraines sampled in Hjemtverrdalen. A. HM1. B. HM2. C. HM3 (see Fig. 4A for location). Showing soil horizons (A- to C-horizon), wet soil colour (using Munsell colour notation), wet soil CDE (following Buntley & Westin 1965), LOI values and soil pH.

down-valley (SM5-SM2), indicating increased concentrations of decomposed plant material in the older soils.

Although it was not possible to establish a full chronosequence in either Hjemtverrdalen or Goahtevággi, the outermost moraines (HM1 and GM1) were sampled at each site, with at least one other recessional moraine, to provide some context of the glacial history in these two valleys. The specific B-horizon characteristics from moraines within Hjemtverrdalen and Goahtevággi are shown in Table 3 and generalized soil profiles are shown in Figs 10, 11. There is a similar trend of deepening soils with distance down-valley (i.e. with increasing moraine relative age; Figs 10, 12), with the outermost moraines (HM1 and GM1) both having maximum soil depths >300 mm. The specific B-horizon characteristics of Hjemtverrdalen and Goahtevággi show a similar range of values to those in Sorbmevággi, with some clear down-valley trends including: a thickening of the B-horizon; a clear and consistent

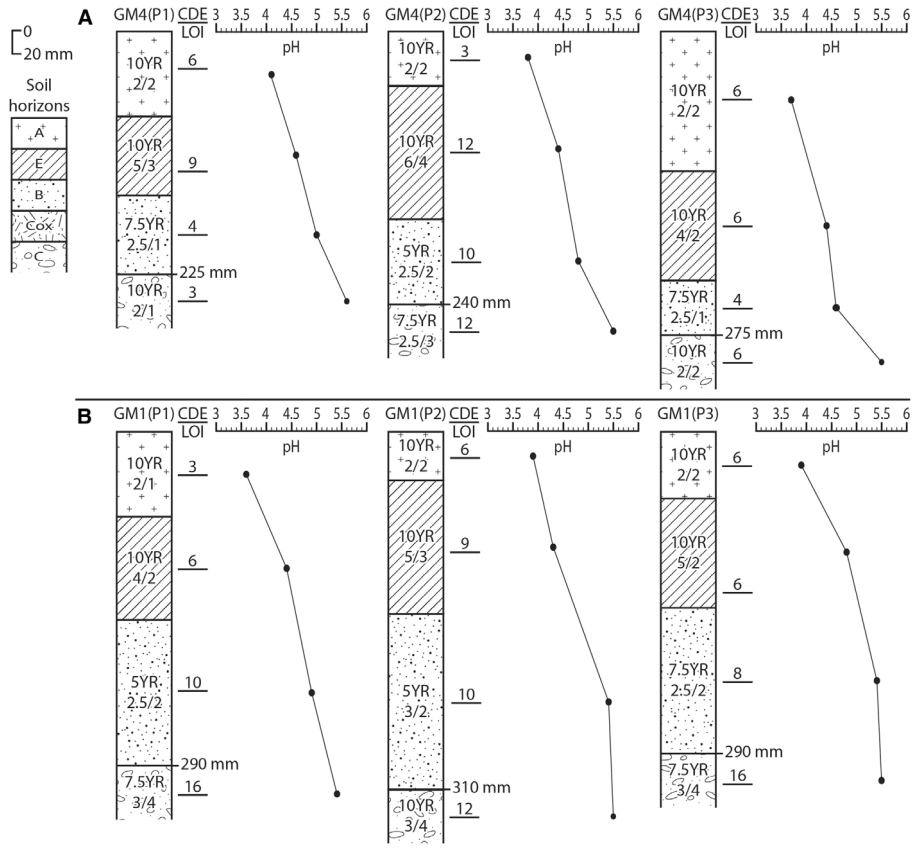

Fig. 11. Soil profiles from each soil pit on the moraines sampled in Goahtevággi. A. GM4. B. GM1 (see Fig. 4C for location). Showing soil horizons (A- to C-horizon), wet soil colour (using Munsell colour notation), wet soil CDE (following Buntley & Westin 1965), LOI values and soil pH.

increase in the CDE (reddening) of wet soils; and decreasing acidity of the B-horizon (all the outermost moraines have pH values >5.0; Table 3).

Overall, there is a clear pattern of increasing soil depth on the moraine crests with distance down-valley (Table 3). Soil deepening is attributable to a thickening of both the E- and B-horizons. Additional soil properties such as pH, organic content and colour do not exhibit any clear trends down-valley. Where boulders are not present on the moraine crest (such as in Goahtevággi), soil chronosequences provide a valuable alternative means of relative age dating, enabling the expansion of geochronological investigations into additional (local) sites.

Establishing Schmidt hammer and soil chronosequence dating calibration curves

Strupskardet: establishing a Schmidt hammer dating calibration curve. – We used the four moraines (M12, M11, M9 and M8) with age control from Strupskardet from Bakke *et al.* (2005b) with the dated LIA moraine from Sorbmevággi from Leigh *et al.* (2020) to develop a Schmidt hammer *R*-value-dating calibration curve. It should be noted that the ages from Bakke *et al.* (2005b) were not directly taken from the moraines but, rather, inferred from signals in the glaciolacustrine sediment core and the reconstructed ELA and glacier size. We used the central estimate of the age ranges provided by Bakke *et al.* (2005b) (i.e. M12 = 9.3–8.9 ka = 9.1 ka) and then explored the shape of the *R*-value–age relationship following the approach of Shakesby *et al.* (2011) and tested three different regression equations: linear, second-order polynomial and logarithmic (Fig. 12). A further limitation of this approach is that the lithologies of the moraines in Strupskardet and Rotsunddalen were different, but we deem our work as a preliminary assessment to develop testable hypotheses alongside our other dating methods and discuss uncertainties below.

All three regression equations showed a good fit to the data ($R^2 > 0.97$) but the second-order polynomial and logarithmic regression plots showed a marginally better fit through the data-points compared with the linear plot (Fig. 12). Furthermore, the second-order polynomial and logarithmic calibration curves showed a slow decline in the rate of *R*-value with age, implying that a small decrease in *R*-value represents an increasingly large time duration, probably owing to a reduction in weathering rates with time (cf. Colman 1981). We therefore chose the logarithmic dating curve (Fig. 12C) to establish

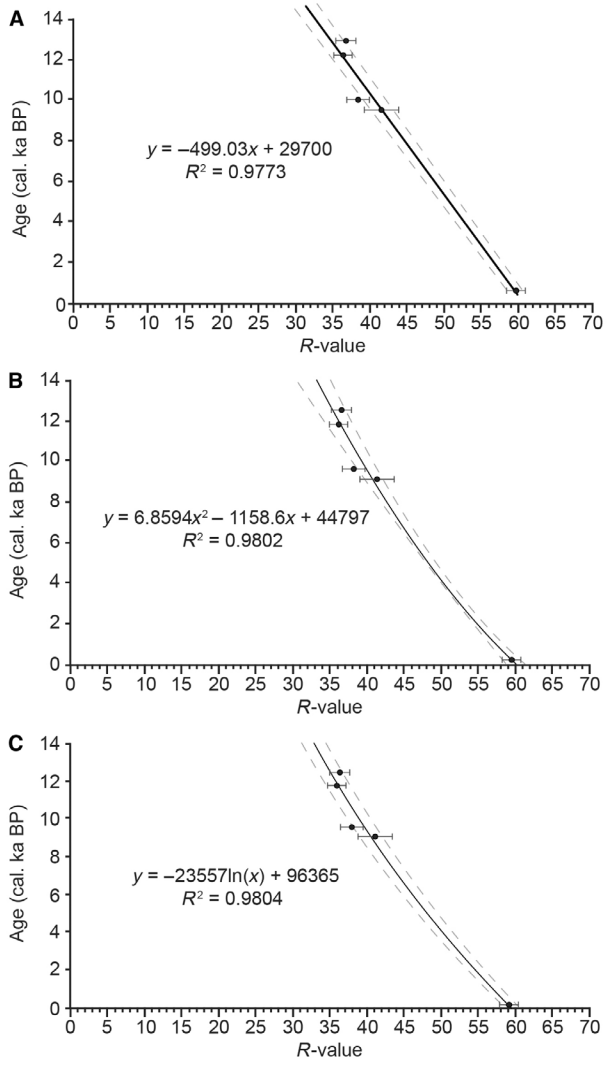

Fig. 12. Schmidt hammer *R*-value-age calibration curves using data collected from four moraines of inferred age in the Strupskardet valley (from Bakke *et al.* 2005b) and the LIA moraine from Sorbmevággi (from Leigh *et al.* 2020): A. linear, B. second-order polynomial, C. logarithmic.

preliminary calibrated ages in Rotsunddalen, simply because it has the highest correlation coefficient (R^2 = 0.98; Fig. 12C), and because other recent Schmidt hammer investigations have argued that *R*-value–age relationships are best represented by logarithmic regression (e.g. Tomkins *et al.* 2018).

Using our logarithmic calibration curve (Fig. 12C), we calculated preliminary calibrated ages and their 95% confidence limits for moraines within Rotsunddalen (Table 4). The resulting ages of the Sorbmevággi moraines revealed a sequence spanning ~6.7 ka, with the outermost moraine (SM1) dating to around 10.6 ka (9587–11 601 years) and the innermost pre-LIA moraine (SM5) dating to around 3.9 ka (3177–4599 years) (Table 4).

Establishing a relative soil chronosequence dating calibration curve. – Using the soil properties recorded from the pre-LIA moraines within Sorbmevággi (SM1–SM5), we attempt to establish a relative soil chronosequence dating calibration curve. Previous work using soil chronosequences has shown that the best parameter for relative age dating is simply soil depth and B-horizon thickness (McCarroll & Ware 1989; Evans 1999). Our data show that the maximum depth to the base of the B-/top of C-horizon is the most consistent value with the greatest correlation between sites (Table 3). We therefore developed curves plotting maximum B-horizon depth and, following Evans (1999), our soil chronosequence calibration curves used a logarithmic regression (Fig. 13).

The results show that the two different soil parameters have the potential to produce different calibrated ages (Table 5). For example, when comparing the outermost moraine, which logically indicates the oldest moraines in each succession, there are only slight differences in the maximum soil data: SM1 has two 330-mm-deep soils, one of which has a 150-mm-thick B-horizon; HM1 has a 345-mm-deep soil and a 145-mm-thick B-horizon; and GM1 has a 310-mm-deep soil and a 120-mm-thick B-horizon (Table 3). The resulting relative calibration for the terminal moraines (when excluding the anonymously shallow soils of SM2) implies that HM1 would have been formed at a similar time to that of SM1 (Table 5), whereas GM1 would be of similar age to SM3. The position in the succession of GM1 indicates that this calibrated age is too young, indicating that the soils on these moraines are anomalously shallow.

TCN dating

The ^{10}Be concentrations and corresponding surface-exposure ages of the samples from Sorbmevággi and the main part of Rotsunddalen are shown in Table 6 and Fig. 14, using both local and global production rates and applying corrections to account for the potential effects of subaerial erosion, snow cover shielding and glacio-isostatic adjustment. Exposure ages range from 11.8±1.0 to 16.5±1.4 ka using the local production rate, and from 10.1±0.7 to 14.1±1.0 ka using the global production rate. We consider the local production rate to better represent nuclide production in northern Norway, and therefore use those resulting ages in this paper. Irrespective of the production rate used, the distribution of ages broadly corresponds to the location of samples, with the oldest ages on the bedrock knoll at the confluence with the main part of Rotsunddalen, and younger ages on the Sorbmevággi moraines. However, there is some scatter of ages both within and between features, indicative of outlier ages.

We applied a series of tests to identify outliers within the TCN dataset (Table 7). First, we performed a reduced chi-squared test (using iceTEA; Jones *et al.* 2019a) for each feature to measure of the goodness of fit between the

Table 4. Tentative Schmidt hammer exposure ages with 95% confidence intervals (CI) generated from the Strupskardet age-calibration curve (Fig. 12C) based on independently dated moraines. Confidence intervals show the positive and negative error resulting from curvilinear regression based on the error of the *R*-value.

Regression equation	Site	Moraine ID	Feature mean *R*-value±95% CI	Calculated age (years BP)	+95% CI (−years)	−95% CI (+years)	Bracketing age
$y = -23557\ln(x) + 96\ 365$	Sorbmevággi	SM5	50.71±1.5	3877	700	722	3177–4599
		SM4	48.99±1.2	4690	582	597	4108–5287
		SM3	41.92±1.3	8362	697	718	7665–9080
		SM2	38.76±1.7	10 208	1010	1055	9198–11 263
		SM1	38.14±1.6	10 588	971	1013	9587–11 601
	Hjemtverrdalen	HM3	42.20±1.3	8205	729	753	7476–8958
		HM2	40.44±2.8	9208	1580	1694	7628–10 902
		HM1	35.73±1.6	12 125	1005	1049	11 120–13 174

weighted mean and the set of exposure ages. Moraines SM1 and SM5, and the knoll (when RV-1921-B was excluded) were found to be a single age population, meaning that a weighted mean and standard deviation can be used to represent each of these features; SM3 and SM4 were not identified as a single population, probably owing to one or more outliers. Next, we performed a two-tailed generalized extreme Studentized deviate test (iceTEA; Jones *et al.* 2019a) to statistically identify which ages were outliers within the features, specifically in cases where there was not a single age population and where there was a sufficient number of samples for the test. No individual ages were identified as outliers (tested with both a 0.01 and 0.05 significance (*p*-value) level). Therefore, we cannot further exclude any samples to improve the estimated exposure ages of these features, and we report the full age range (at 1σ) for SM3 and SM4. Based on these tests, the bedrock knoll was exposed at 16.3±0.2 ka, SM1 at 15.3±1.0 ka, SM3 at 11.3–15.8 ka, SM4 at 11.3–15.0 ka and SM5 at 15.4±0.1 ka (Table 7). These ages are much older than those derived from the Schmidt hammer age calibration (Table 4) and from recent syntheses of the regional deglaciation history (Hughes *et al.* 2016; Stroeven *et al.* 2016). We also note that potential corrections for erosion, snow cover and glacio-isostatic adjustment tend to make the age distribution even older (discussed below).

Finally, we evaluated the stratigraphic relationship of the exposure ages between each feature. The bedrock knoll should be oldest, reflecting thinning of ice at higher elevations in Rotsunddalen, and then the moraines should get progressively younger from SM1 to SM5, recording glacier retreat up valley in Sorbmevággi. All features are stratigraphically consistent, apart from SM5, which is statistically older than the outer SM4 moraine, although not significantly older than SM1 and SM3. SM5 contained large angular boulders that: (i) could be sourced from the valley sides, possibly associated with a nearby rock slope failure or as supraglacial debris; or (ii) may have undergone insufficient glacial erosion in the upper part of the valley to reset the ^{10}Be concentration prior to glacier retreat. In these situations, SM5 would record exposure ages older than the timing of moraine deposition and glacier retreat (Applegate *et al.* 2010; Heyman *et al.* 2011). Alternatively, if the relationship to SM4 is ignored, the moraine ages are consistent with glacier retreat from SM1 to SM5 that occurred within the uncertainty of moraine age estimates.

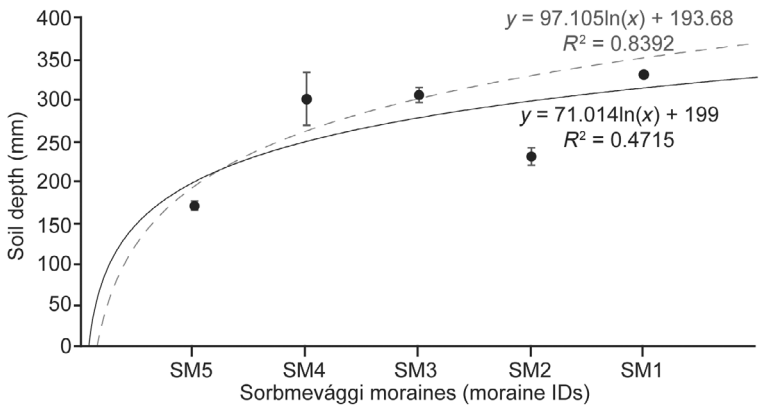

Fig. 13. Soil chronosequence calibration curves using maximum soil depth collected from moraines within Sorbmevággi and a logarithmic curve. The solid black line is a curve fitted to all the data points whereas the dashed grey line is a curve that excludes the anomalously shallow soil data from SM2.

Table 5. Results of soil chronosequence relative moraine dating using mean soil thickness and mean soil depth logarithmic calibration curves. The final column shows the calibrated 'age' relative to the Sorbmevággi moraine succession from which the dating curve is based; a relative age of 1.1 would indicate the moraine is of similar age to the SM1 moraine but does not correspond exactly, and an age of 1.5 would indicate the moraine was formed in between the formation ages of SM1 and SM2. The emboldened relative ages are considered most representative of relative moraine age.

Curve type	Site	Moraine ID	Maximum B-horizon depth (mm±95% CI)	Relative age in relation to moraines SM1–SM5
Soil depth (all moraines; Fig. 9B, solid black line)	Hjemtverrdalen	HM3	285±32	2.6
		HM2	290±40	2.4
		HM1	345±45	<1
	Goahtevággi	GM4	275±29	1.2
		GM1	310±13	3.1
Soil depth (no SM2; Fig. 9B, dashed grey line)	Hjemtverrdalen	HM3	285±32	**3.4**
		HM2	290±40	**3.3**
		HM1	345±45	**1.2**
	Goahtevággi	GM4	275±29	**3.7**
		GM1	310±13	**2.7**

Discussion

Rotsunddalen glacial chronology and links with Holocene climatic events

Despite important limitations and large uncertainties (discussed below), the preliminary moraine ages using the Schmidt hammer dating curve appear to indicate a sequence of glacial events, from the Younger Dryas (HM1, ~12.1 ka; Table 4) throughout the Holocene to the early-Neoglaciation (SM5, ~3.9 ka; Table 4, Fig. 15) that is broadly consistent with previous work on mountain deglaciation following the retreat of the Fennoscandian Ice Sheet across Norway (e.g. Nesje *et al.* 2008; Nesje 2009). However, the chronology from TCN dating is not consistent with either the Schmidt hammer chronology (Fig. 15) or the regional-scale widely accepted deglaciation history (Bakke *et al.* 2005b; Hughes *et al.* 2016; Stroeven *et al.* 2016), instead indicating thinning of ice to elevations below ~380 m a.s.l. in Rotsunddalen at ~16.3 ka and glacier retreat in this location by ~15.4 ka (SM5) or 11.3–15.0 ka (SM4), when the ice-sheet margin is known to have been in the outer fjord areas (Hughes *et al.* 2016). We therefore set aside the TCN results when interpreting Rotsunddalen glacial chronology and then discuss the potential reasons for erroneously old TCN ages below.

Younger Dryas–Holocene transition. – Throughout the Kåfjord Alps, large heavily vegetated moraines at the foot of subsidiary valleys have been mapped (Leigh *et al.* 2021) and these correspond with the outermost moraines in Rotsunddalen succession, HM1, SM1 and GM1 (Fig. 4). If correct, the Schmidt hammer exposure ages would indicate that the Hjemtverrdalen terminal moraine (HM1) formed at around 12.1 ka

Table 6. TCN ^{10}Be concentrations and exposure ages from samples within Sorbmevággi and the main part of Rotsunddalen, using both global and local production rates (PR), together with additional corrections for bedrock erosion, snow shielding and glacio-isostatic adjustment.

Feature	Sample name	Accelerator mass spectrometer ID	^{10}Be (atoms g^{-1})		Age (years; global PR)		Age (years; local PR)		Age (years; erosion correction)		Age (years; snow correction)		Age (years; GIA correction)	
			Mean	1σ	Mean	1σ[1]	Mean	1σ[1]	Mean	1σ[1]	Mean	1σ[1]	Mean	1σ[1]
Knoll	RV-19-18B	b12436	89 300	4500	14 060	1040	16 500	1440	16 280	1200	17 660	1310	14 770	1510
Knoll	RV-19-20B	b12437	85 400	2700	13 800	860	16 180	1260	15 920	1000	17 360	1090	14 460	1350
Knoll	RV-19-21B	b12438	66 100	2100	10 690	680	12 560	980	11 930	760	13 460	850	10 970	1060
SM1	RV-19-15M	b12431	72 100	2700	13 700	900	16 080	1290	15 790	1040	17 240	1130	14 370	1370
SM1	RV-19-17M	b12433	66 900	3900	12 040	960	14 130	1300	13 620	1080	15 140	1200	12 440	1310
SM3	RV-19-09M	b12427	63 500	2500	11 630	780	13 650	1110	13 100	880	14 740	990	11 990	1110
SM3	RV-19-10M	b12429	68 600	3000	12 340	860	14 480	1210	14 000	970	15 590	1090	12 770	1260
SM3	RV-19-11M	b12430	70 500	2300	13 000	820	15 250	1190	14 860	940	16 450	1040	13 540	1260
SM3	RV-19-16M	b12432	56 800	3200	10 200	810	11 980	1090	11 320	900	12 900	1010	10 410	1040
SM4	RV-19-05M	b12425	67 500	2500	12 320	810	14 470	1160	13 980	920	15 580	1020	12 770	1210
SM4	RV-19-07M	b12426	55 400	2300	10 080	690	11 840	980	11 160	770	12 780	870	10 280	940
SM5	RV-19-01M	b12423	71 600	2700	13 040	860	15 300	1240	14 910	990	16 550	1090	13 610	1320
SM5	RV-19-04M	b12424	74 800	2400	13 150	830	15 440	1210	15 070	950	16 670	1050	13 710	1290

[1]Total uncertainty, inclusive of measurement and production rate uncertainties.

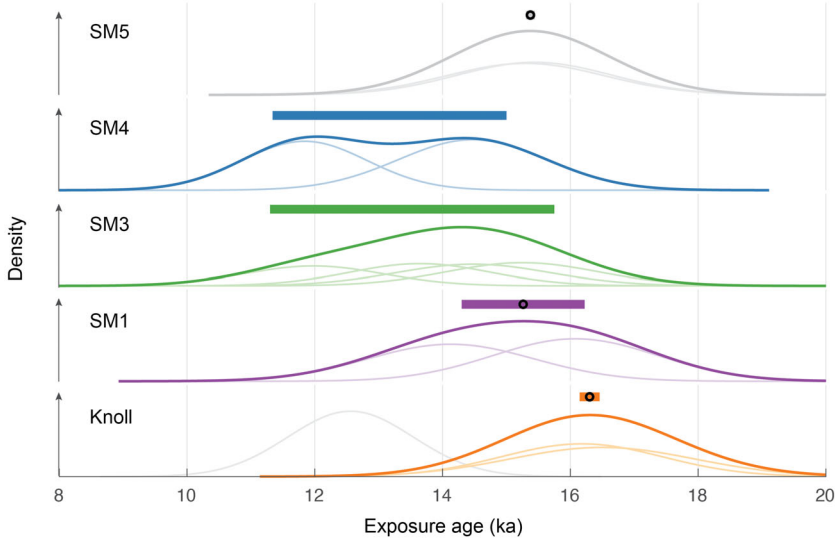

Fig. 14. Terrestrial cosmogenic nuclide exposure ages for Sorbmevággi and the main part of Rotsunddalen, shown as kernel density estimates with features stacked from the outermost (and highest) at the bottom to the innermost at the top. Individual sample ages (Table 6) are denoted by thin lines and a summed density estimate for each feature is denoted by bold lines. Samples excluded through statistical and stratigraphic assessment of the ages (Table 7) are shown in grey. Black circles (Knoll, SM1, SM5) represent the weighted mean with the horizontal bar representing the corresponding standard deviation (1σ); horizontal bars without black circles (SM3, SM4) show the full age range (minimum to maximum at 1σ).

(11.1–13.2 ka) and the Sorbmevággi terminal moraine (SM1) formed at around 10.6 ka (9.6–11.6 ka) (Table 4, Fig. 15). Although the HM1 moraine apparently formed ~1500 years earlier than the equivalent SM1 Sorbmevággi moraine, there are large uncertainties with the Schmidt hammer ages and considerable overlap in the 95% confidence intervals (Table 4). We therefore hypothesize that the terminal moraines HM1 and SM1 represent a similarly timed moraine-forming event, sometime during the late-YD. This inference is further supported by the soil chronosequence data, which show that both moraines have similar maximum soil depths and B-horizon thicknesses (Table 3). However, some asynchronicity might be expected between the two valleys, given the smaller catchment area of Hjemtverrdalen (~2 km^2) compared with the neighbouring Sorbmevággi (~8 km^2). A further consideration is the higher elevation and more exposed position of HM1, which might have resulted in enhanced weathering and hence lower *R*-values and greater rates of soil development than on moraines of comparable age in more sheltered positions.

Our hypothesis of a late-YD glacial maximum in Rotsunddalen is supported by other studies from the region and across Norway. In northernmost Norway, surface exposure dating of major end moraines in eastern Finnmark is consistent with a YD age of around ~11.9±1.2 ka (Romundset *et al.* 2017) and several YD moraines have been associated with the oscillatory retreat of Langfjordjøkulen ice cap, around 70 km NE of our study area. Similarly, in western Norway, reconstructions of the Fennoscanian Ice Sheet have noted that the YD maximum was not achieved until ~11.6 to 11.7 ka, with ice retreat initiating ~11.5 ka (e.g. Bondevik & Mangerud 2002; Lohne *et al.* 2012; Mangerud *et al.* 2016). Bakke *et al.* (2005b) also suggested that, contrary to the cold and dry climate during the period 13–12.6 ka (Birks 1994; Rea & Evans 2007),

Table 7. Assessment of TCN exposure ages by feature.

Feature	Outlier test		Weighted mean		Full range (1σ)		Features in stratigraphic order?
	Reduced chi-squared	Generalized extreme Studentized deviate test	Mean (ka)	1σ (ka)	Minimum (ka)	Maximum (ka)	
Knoll	Single population[1]	No outliers found	16.30[1]	0.16	–	–	Yes
SM1	Single population	N/A[2]	15.26	0.96	–	–	Yes (consistent)
SM3	Not a single population	No outliers found	–	–	11.30	15.75	Yes (consistent)
SM4	Not a single population	*Not possible*	–	–	11.34	15.00	Yes (consistent)
SM5	Single population	N/A[2]	15.38	0.07	–	–	No (older than SM4)

[1]Excluding RV-1921-B.
[2]Not necessary as a single population.

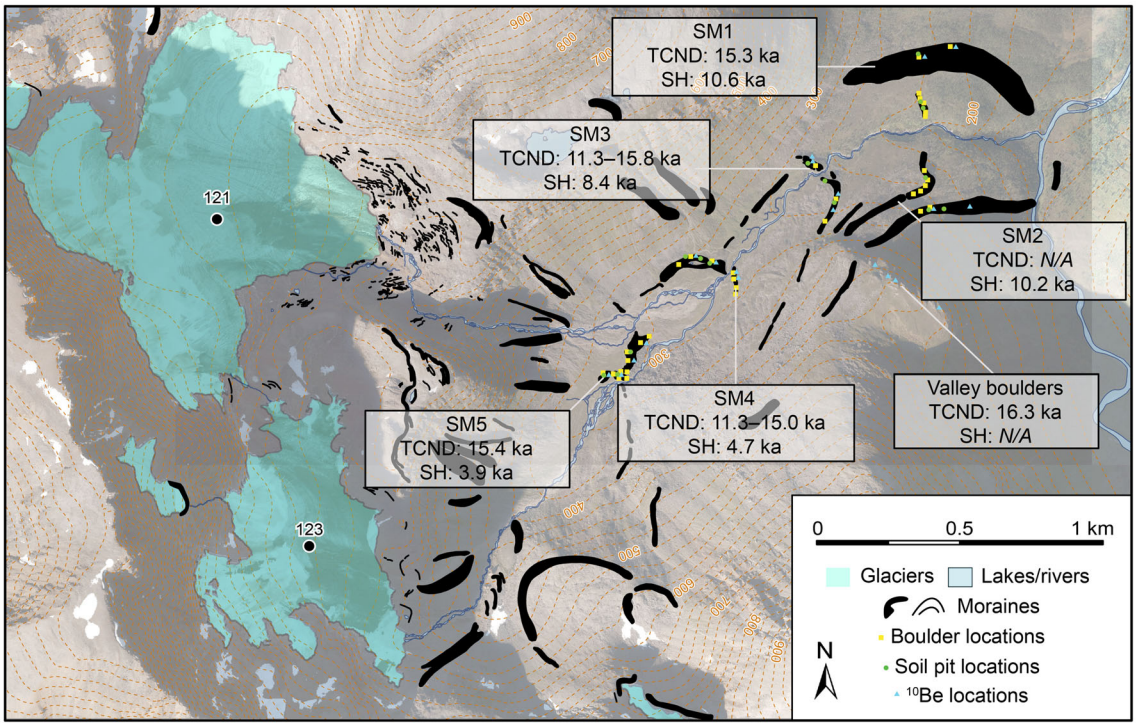

Fig. 15. Summary of moraine ages in Sorbmevággi and the main part of Rotsunddalen from calibrated Schmidt Hammer (SH) values and TCN dating using the local production rate (see Tables 6, 7).

the climate of northern Norway was ameliorating by the late-YD, which may have resulted in increased precipitation and glacier growth/stabilization (Jansen *et al.* 2023). This climatic amelioration resulted in the lowering of the ELA on the Lyngen Peninsula to around ~620 to 650 m a.s.l., around 350 m lower than at present day (Bakke *et al.* 2005b). Given the evidence of a late-YD increase in precipitation relative to that of the early-YD across the Lyngen Peninsula (cf. Bakke *et al.* 2005b), it is highly likely that conditions would have also been more favourable for glacier growth across the central Troms and Finnmark region, consistent with our hypothesis of the timing of Rotsunddalen YD maximum and the large SM1, HM1 moraines (Figs 4, 15).

Early Holocene. – If correct, the Schmidt hammer ages for SM2 and HM2 (Figs 4, 15) indicate an Early-Holocene moraine forming event between around 10.2 ka (9.2–11.2 ka) and 9.2 ka (7.6–10.9 ka) for SM2 and HM2, respectively (Table 4). The overlap in moraine ages around 10–9 ka corresponds to the Norwegian Erdalen Event (e.g. between 10.1 and 9.7 ka; Andersen 1980; Corner 1980; Nesje *et al.* 1991; Dahl *et al.* 2002). At this time, summer temperature reconstructions from southern Norway have shown temperatures approximately 1.5 °C lower than those of the early 21st century and with enhanced precipitation, such that winter precipitation levels were nearly twice those of the early-21st century, allowing glaciers to expand for a short duration (Dahl *et al.* 2002). Reconstructions of ELAs during the period ~10 to 9 ka also suggest that, relative to the present-day, ELAs underwent a maximum lowering of ~205 m at Hardangerjøkulen, southern Norway (Dahl & Nesje 1996), ~230 m at Nigardsbreen, SW Norway (Dahl *et al.* 2002), ~120 m at Austre Okstindbreen, northern central Norway (Bakke *et al.* 2010), and as much as ~354 m at Strupskardet, northern Norway (Bakke *et al.* 2005b). Despite limitations of the Schmidt hammer method, therefore, the ages of the SM2 and HM2 moraines are entirely consistent with other Erdalen Event moraines.

Up-valley from the Erdalen Event moraines in the Sorbmevággi and Hjemtverrdalen succession, the SM3 and HM3 moraines located at the individual valley heads (Fig. 4) show remarkably similar calibrated ages and are dated to 8.3 ka (7.7–9.0 ka) and 8.2 ka (7.5–9.0 ka), respectively (Table 4). If correct, this would indicate that SM3 and HM3 moraines were formed around the time of the rapid, but short-lived, climatic deterioration during the 8.2 ka event, which is typically correlated with the Finse Event (8.5–8.0 ka) in Scandinavia (Nesje *et al.* 2008). During the interval 8.2–7.9 ka, pollen stratigraphy from western Norway indicates that maritime areas experienced wetter conditions (Nesje *et al.* 2006; Balascio & Bradley 2012). At the same time, speleothem temperature reconstructions from Søylegrotta, northern Norway, indicate a notable temperature reduction centred around 8.2 ka (Lauritzen &

Lundberg 1999) and Norwegian Sea sea-surface temperature reconstructions suggest a ~3 °C surface cooling (Risebrobakken *et al*. 2003). In northern Norway, these temperature and precipitation changes have been linked to a large glacier advance at Leirdalsbreen, an outlet glacier of the Høgtuvbreen ice cap in the Svartisen area (Jansen *et al*. 2016). Jansen *et al*. (2016) also noted that the maritime setting of the Høgtuvbreen ice cap enabled a readvance around this time, owing to the abrupt precipitation increase resulting in a ~300-year period with an ELA that was ~140 m lower than present. More recently, a readvance shortly after 8.5 ka has also been correlated with the 8.2 ka Finse Event at Grovabreen in western Norway (Aa & Sønstegaard 2019), linked to climate deterioration around this time.

Given the limitations of our Schmidt hammer dating (see below), our interpretation of a possible 8.2 ka event moraine in the central Troms and Finnmark region is highly speculative and requires further testing. Indeed, previous studies documenting Holocene glacier recession in northern Norway have not found moraines or other glacial features attributable to this event (e.g. Bakke *et al*. 2005b), although Wittmeier *et al*. (2015) acknowledged the possibility of a glacier reforming around this time. There are, however, several key differences between the studied glaciers of Bakke *et al*. (2005b) and Wittmeier *et al*. (2015) which, when compared with Rotsunddalen, might provide some explanation for the apparent disparity in moraine sequences. Firstly, Rotsunddalen glaciers are smaller in size, taking on the form of Alpine style small mountain glaciers, which are known to have simpler and faster response times to climatic perturbations than those of larger and more complex outlet glaciers from ice caps and mountain icefields (e.g. Jóhannesson *et al*. 1989; Bahr *et al*. 1998; Klingbjer *et al*. 2005). In northern Sweden, smaller valley glaciers have been shown to have response times of a few decades, with glaciers experiencing marked readvance as a response to climatic deterioration on timescales of <100 years (Klingbjer *et al*. 2005). Indeed, Matthews & Winkler (2011) noted the scarcity of moraines dated to the Finse Event, perhaps owing to the short-lived nature of the 8.2 ka climatic deterioration, but argued that if moraines of this age are to be found, they are most likely to be in front of very small glaciers with a short reaction time. Secondly, glaciers in our study are found in narrower and steeper alpine valleys and the moraines in question are at higher elevations (SM3 at ~260 m a.s.l. and HM3 at ~380 m a.s.l.), indicating that both topography and local ELA may be a contributing factor. For example, a minor lowering of the ELA may have enabled the small alpine glaciers of Rotsunddalen to readvance while the larger icefields/ice caps and their outlet glaciers required a greater ELA depression to enable substantial readvance (Rosqvist & Østrem 1989). Finally, the steep valley walls may have increased debris supply to the glacier surface and provided ample material for moraine formation. Indeed, proximal to and in contact with SM3, and within a similar position in Goahtevággi, are broad areas of DDA (Leigh *et al*. 2021), indicative of high debris supply at the ice margin (Evans 2008; Vacco *et al*. 2010). Despite these arguments, our age assignment is largely based on Schmidt hammer dating, which is subject to large uncertainties. Thus, we view this possible correlation with the 8.2 ka event as a testable hypothesis, rather than a robust finding of our study.

Late Holocene (Neoglaciation). – After the Early Holocene, no moraines appear to have developed within Sorbmevággi for a period of ~3700 years, probably representing substantial glacier recession (probable disappearance) during the warm period culminating in the HTM (6.6–6.3 ka; Nesje 2009). Subsequently, any evidence of glacier regrowth at the start of the Neoglaciation will only be preserved if it was more extensive than the much more recent LIA limit. The apparent formation of SM4 at ~4.7 (4.1–5.3) ka and SM5 at ~3.9 (3.2–4.6) ka (Table 4), most likely indicates glacier advance or regrowth following the onset of Neoglaciation in northern Norway. Furthermore, the relative age of GM4, as shown by the soil depth (Table 5), indicates that this moraine was formed at a similar time to SM4, or perhaps slightly before. Again, despite the limitations of the Schmidt hammer method, these ages (and relative successions) fit with the known pattern of millennial-scale events across Scandinavia during the Late Holocene, with two such events having occurred ~4.8 to 3.9 and ~3.2 to 2.6 ka (Matthews & Dresser 2008).

If correct, the apparent ages of ~4.7 ka for SM4 and ~3.9 ka for SM5 (Table 4) are, perhaps, slightly earlier and more extensive than compared with other readvances in this region around this time. For example, at the nearby Langfjordjøkelen ice cap on the Bergsfjord peninsula, lacustrine sediments indicate no glacier activity in the catchment until ~4.1 ka (Wittmeier *et al*. 2015), with glacier activity increasing until an apparent maximum during the LIA. Conversely, at other sites in northern Norway, such as the Høgtuvbreen ice cap in Nordland County (66°25′N, 13°39′E), a distinct 120-year glacier readvance has been reported at ~4.4 ka which is suggested to indicate the start of Neoglaciation (Jansen *et al*. 2016). There are even earlier Neoglaciation events reported further south at Austre Okstindbreen in Nordland County (66°00′N, 14°16′E). Radiocarbon dating of buried soils and subsequent dating of lacustrine sediments indicates Neoglaciation initiating as early as 5 ka with a period of heightened glacier activity ~4.5 ka (Griffey & Worsley 1978; Bakke *et al*. 2010). Furthermore, on the south-eastern coast of Vestvågøya, northern Norway, lake sediment records have been used to indicate temperature decrease initiating ~4.8 ka with a marked increase in precipitation after ~4.3 ka (Balascio & Bradley 2012). Taken together, this

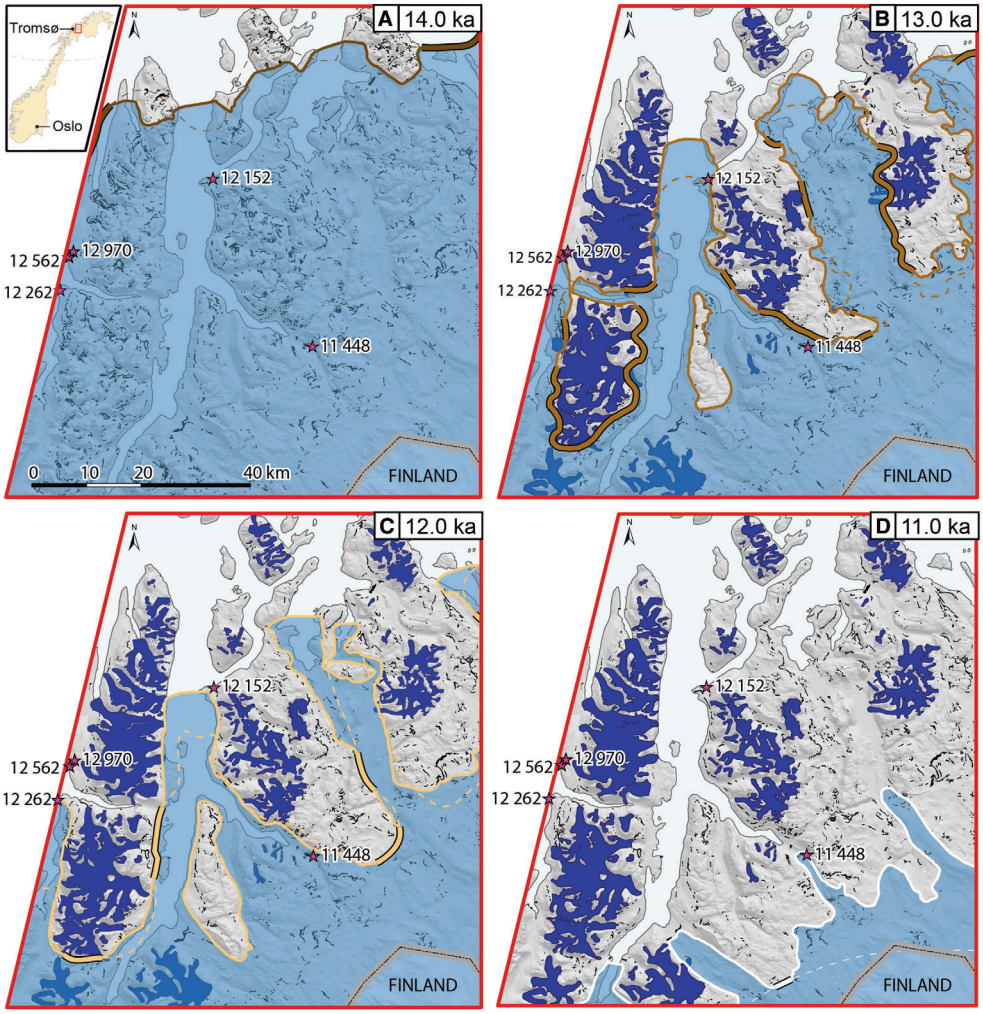

Fig. 16. Revised ice-sheet margin positions of the Scandinavian Ice Sheet from 14 000 to 11 000 cal. a BP and glacier reconstructions during the Holocene in the central Troms and Finnmark region of Northern Norway. The thick two-tone solid line and thin dashed line represents the unedited most credible ice-sheet margin from Hughes *et al.* (2016) while the thin solid line and solid blue infill represents the revised margin and ice extent. Revised ice-sheet margins and new glacier outlines are based on the mapping of Leigh *et al.* (2021) and new chronological data from this paper.

evidence suggests that glacier regrowth/readvance in maritime northern Norway occurred soon after 5 ka. However, given the limitations of our Schmidt hammer dating, we view this as a tentative hypothesis that requires further testing.

Similar studies in northern Sweden, while less extensive than those of Norway, provide a valuable reference to the onset of Neoglaciation across northern Scandinavia. Karlén (1988) and Karlén & Kuylenstierna (1996) documented notable cold events and glacial readvances between 5.1 and 4.2 ka, which were linked with Dansgaard–Oeschger events and a reduction in northerly heat transport. Advanced glacier positions at around 4.3 and 3.1 ka are also inferred from lake sediments in northern Sweden (Rosqvist *et al.* 2004). Furthermore, in maritime western Norway, lacustrine sediments from Ålfotbreen (61°44′N 05°36′E) were used to propose initial Neoglaciation activity as early as ~5.4 ka (Gjerde *et al.* 2016). In contrast, in a more continental setting, the high-frequency glacier fluctuations at Hardangerjokulen (60°33′N, 7°25′E) are proposed to have started ~4.8 ka (Dahl & Nesje 1994). Thus early Neoglaciation (re)advances are not necessarily isolated to the maritime regions of northern Norway but instead appear to be characteristic of mountain glaciers across northern Scandinavia.

As noted, the specific glacial characteristics of Rotsunddalen glaciers may have enabled them to react quickly to short-term climatic deterioration (Ivy-Ochs *et al.* 2009) and, in turn, exceed the maximum positions during the LIA, which is often considered to represent Neoglaciation maxima for larger glaciers across Norway (e.g. Matthews 1991; Dahl *et al.* 2002; Winkler 2003; Nesje 2009).

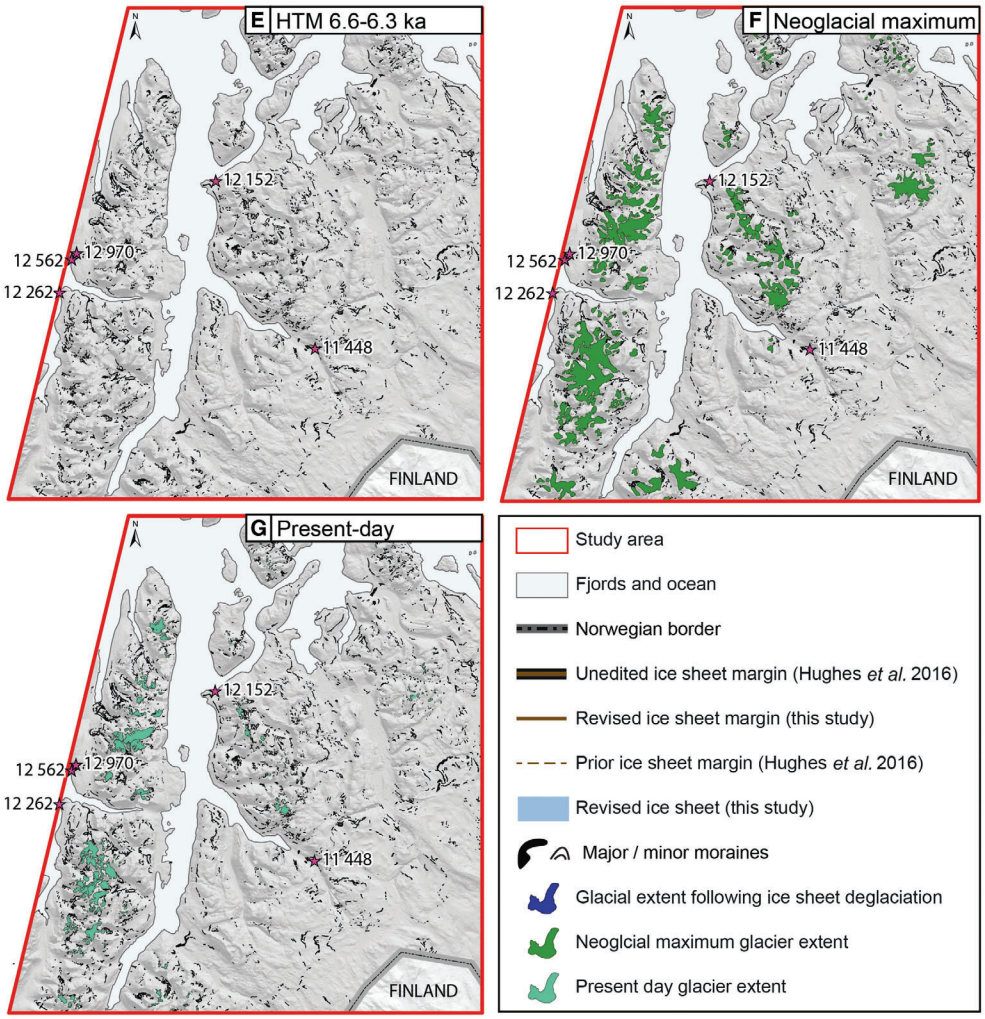

Fig. 16. (Continued)

Ice-sheet margins and Holocene glacier reconstructions of the central Troms and Finnmark region: patterns of advance/retreat

Combining the detailed mapping of Leigh *et al.* (2021) with our tentative moraine chronology from this study and that of Strupskardet (Bakke *et al.* 2005b) allows us to reconstruct the pattern of ice-sheet deglaciation and mountain glacier fluctuations at key time steps during the Holocene from 14 ka to present (Fig. 16). Given the wealth of geomorphological data (Leigh *et al.* 2021) and the high temporal resolution of our moraine chronology, we are able to build on and extend the 'most credible' outlines from Hughes *et al.* (2016) and reveal a more complex pattern of ice-margin retreat whereby ice-sheet retreat to the SE led to the 'unzipping' of the ice margin and the isolation of several large plateau icefields and outlet glaciers in the study area, followed by notable fluctuations during the Holocene. This succession can be summarized as follows:

- Around 14.0 ka (Fig. 16A) the mainland and most of the outlying islands appear to have been covered by ice, with only the northernmost portion of the Lyngen Peninsula, the Maurn Peninsula and the Kvænangstinden massif remaining ice free. We propose that the ice sheet separated around the Maurn Peninsula, flowing through the trough at Hamneidet and entering the Maursundet strait where it abutted the southern margin of Kågen.
- Around 13.0 ka (Fig. 16B) the ice-sheet margin is redrawn to show large outlet glaciers filling greater portions of the fjords and aligning with the higher moraine systems that track the length of the fjords and valleys (Leigh *et al.* 2021), although Rotsunddalen

and the Riehppe plateau are shown to be isolated from the ice sheet. On the plateau east of Reisadalen, the ice margin appears more dynamic, with the emergence of small lobes and ice tongues recorded by large lobate moraines (e.g. Fig. 3I, J). Revised ice front positions are supported by the dating of sedimentary deposits near Svensby in Ullsfjord which give ages of 12.6 and 13.0 ka (Andersen 1968; Plassen & Vorren 2003). At this time step, we show the first emergence of plateau icefields across the higher terrain, separated from the ice sheet in the lowlands (e.g. the Lyngen Peninsula, the Riehppe plateau, parts of the Kåfjord Alps and Kvænangstinden massif). Several of these icefields produced large outlet glaciers, as evidenced by large moraines at, or just beyond, their valley mouths (e.g. Fig. 3K, L).

- Around 12.0 ka (Fig. 16C) the margin has again been remapped further down the fjords than depicted in Hughes *et al.* (2016), notably with positions at Skarmunken in Ullsfjord, Spåkenes in Lyngenfjord, and at Straumfjordnes and Bakkeby in Resiafjord. This is based on a series of moraines that can be traced around the mountains of Ajit (one of the county's northernmost summits over 1400 m outside of the Lyngen Alps and ~10 km east of Skibotn) (Leigh *et al.* 2021). We propose that the mountain tops here may have been ice free at this period, possibly emerging as nunataks within the main ice sheet at ~13.0 ka or earlier (Fig. 16B, C). Revised ice-front positions are supported by a range of radiocarbon dates from sedimentary deposits, with dates of 10.8 ^{14}C ka BP (12.3 ka) at Skarmunken (Nydal 1960; Andersen 1965) and 10.7 ^{14}C ka BP (12.2 ka) at Spåkenes (Nydal 1960; Andersen 1965).
- Around 11.0 ka (Fig. 16D) we propose revisions to the ice-margin positions in Hughes *et al.* (2016), with glacier outlets occupying the head of Storfjord, the entrance to Skibotndalen, mid-way up Buntadalen, and ~30 km up Reisadalen (near the town of Sappen), with large parts of the inland plateau area to the south/SE remaining ice covered. We also suggest a revision of the margin to skirt around the southernmost edge of the Lyngen Peninsula and probably terminating near the head of Blasfjord. North-west of the large lake Guolasjávri (at the head of the Kåfjord valley), there lies a series of at least three inset arcuate moraines (Fig. 3G, H). There is no age control on these features, so the 11.0 ka ice front position is tentatively drawn along the outermost moraine ridge. More generally, revised ice front positions are supported by a range of radiocarbon dates from sedimentary deposits with dates of 10.3 ^{14}C ka BP (11.5 ka) at Birtavarre (Nydal 1960) and 10.0/9.6 ^{14}C ka BP (11.0/10.4 ka) within Blasfjord (Forwick & Vorren 2002). The southernmost margins of the Lyngen Peninsula and mountains to the east had been exposed at this time step, revealing a similar pattern of small mountain plateau icefields. All of these glaciated sites are defined by large latero-frontal moraine systems extending along valley sides and out beyond the confines of the main valleys, which are now inset with extensive sequences of well-defined recessional moraines (e.g. Fig. 3K, L) and distinct areas of ice-moulded bedrock and till sheets in the upper and lower reaches, respectively.
- During the HTM between around 6.6 ka and 6.3 ka (Fig. 16E) the fate of the glaciers in the region is largely unknown owing to more recent advances over-riding geomorphological evidence. Did all the glaciers melt completely or were the high mountains and elevated plateaus areas a refuge for smaller ice masses? As noted earlier, most glacier reconstructions indicate complete deglaciation in northern Norway, including the studies of Bakke *et al.* (2005b) within Strupskardet (northern Lyngen) and Wittmeier *et al.* (2015) at Landfjordjøkelen (Bergsfjord Peninsula). However, in Nordland county (bordering the Arctic Circle at 66°00′N, 14°16′E), Bakke *et al.* (2010) suggest that substantially reduced glaciers may have survived the HTM at the highest elevations and with regional ELAs at 600–1500 m a.s.l. Given that the topography within our study area rarely exceeds 1600 m a.s.l. (the highest peak is Jiekkevarre (1833 m a.s.l.) on the central Lyngen Peninsula), it is likely that very few glaciers would have survived and only at the very highest elevations.
- The maximum extent of Neoglaciation conditions (Fig. 16F) is reconstructed using our tentative moraine ages from Rotsunddalen, whereby several moraines outside of the LIA maximum were dated to around 4.7–3.9 ka, which departs somewhat from previous work and is a hypothesis that future work could test. We reconstruct the glacier extent based on moraines up to around 600 m distal to LIA moraines (Leigh *et al.* 2020; Weber *et al.* 2020). In cases where no moraines occur immediately outside the LIA margins, the Neoglaciation maximum is represented by the LIA maximum moraines, dated to between AD 1814–1877 in Rotsunddalen and as late as AD 1920–1930 on the Lyngen Peninsula (Ballantyne 1990; Leigh *et al.* 2020). Mapping indicates that Neoglaciation was dominated by mountain valley glacier systems, and only in areas where valley heads connect with mountain plateaus (on southern Lyngen centred around Jiekkevarre; north of Kåfjord at the locality of the present-day Noammerjiehkki ice cap; and on the Riehppe plateau) were these valley systems probably connected to and supplemented by the small plateau icefields. Within some valleys, reconstructed glaciers covered areas that host present-day rock glaciers situated on the valley floor and proximal to LIA moraines, and sometimes connected to present-day glacier margins. In turn, this indicates that many of the valley floor rock glaciers mapped throughout

the region (Leigh *et al.* 2021) were probably formed during the Middle to Late Holocene, when permafrost degradation may have been widespread and when rockfall rates were heightened owing to the destabilization of valley sides that followed the complete or near-complete deglaciation of the Middle Holocene (cf. Palacios *et al.* 2021; Tanarro *et al.* 2021). These interpretations are supported by the earlier works of Whalley (1976), Griffey & Whalley (1979) and Whalley (1992), who investigated rock glaciers on the Lyngen Peninsula and concluded that they were formed in the Late Holocene, often with their impressive size being attributable to higher rock debris input than the small glaciers could have provided entirely subglacially.

- Present-day glaciation across most of the central Troms and Finnmark region is dominated by isolated cirques and rapidly shrinking ice caps (Fig. 16F); only on the Lyngen Peninsula are larger (several kilometres long) valley glaciers still found. Recent glacier change assessments from northern Norway indicate rapid recession since the mid-20th century, with some of the highest known rates of glacier shrinkage across the whole of mainland Norway (e.g. Giesen *et al.* 2014; Stokes *et al.* 2018; Andreassen *et al.* 2020, 2022; Weber *et al.* 2020). There are predictions that many glaciers will not survive beyond the mid- to late-21st century (Stokes *et al.* 2018; Leigh *et al.* 2020; Weber *et al.* 2020; Rounce *et al.* 2023).

Reliability of Schmidt hammer dating, inconsistent TCN exposure ages and regional implications for TCN dating

The TCN exposure ages indicate a broadly coherent timing of glacier thinning and retreat from the main part of Rotsunddalen to inner Sorbmevággi when considered in isolation (Fig. 14). However, this glacier chronology is not consistent with either the Schmidt hammer dating or the widely established regional deglaciation history (Hughes *et al.* 2016; Stroeven *et al.* 2016) (Figs 15, 16). Comparing the two dating methods (e.g. Fig. 15), moraine SM1 was formed ~15.3 ka years ago according to the TCN dating, ~4700 years before that indicated by Schmidt hammer dating; SM4 was formed at the latest ~11.3 ka according to TCN dating, ~6600 years earlier than the Schmidt hammer ages; and, if the TCN ages are accepted for SM5, the moraine was formed ~15.4 ka, ~11 500 years older than Schmidt hammer dating. Based on this comparison, it could be argued that the Schmidt hammer ages are incorrect, as this is a relative dating approach, with the age estimates heavily dependent on assumptions associated with its calibration to independently dated moraines (Fig. 12), as opposed to the more established radiometric dating technique using TCN (Balco 2020; Schaefer *et al.* 2022). Indeed, we acknowledge that there are important limitations with the moraine ages derived from our Schmidt hammer dating. Firstly, the independent age control on the moraines in Strupskardet (from Bakke *et al.* 2005b) was not directly taken from the moraines but, rather, inferred from radiocarbon dating of a glaciolacustrine sediment core and the reconstructed ELA and glacier size. Secondly, our sampling strategy was perhaps suboptimal in that we acquired relatively small sample sizes (100 *R*-values) from each moraine and may have oversampled non-representative boulders (Matthews & Winkler 2022). Thirdly, the lithology of the moraine boulders was different between Rotsunddalen and Strupskardet and this probably introduced the largest uncertainty when constructing our Schmidt hammer *R*-value age calibration curve (Fig. 12), albeit unavoidable given that the moraines in Strupskardet were the only Early Holocene moraines in the study area that had been independently dated. Despite these limitations, however, the results are remarkably consistent between valleys and show an expected down-valley decrease in *R*-value, with statistical tests revealing significant differences between most moraine pairs (see above). Furthermore, the moraine ages are, in general, remarkably consistent with previous work in the wider region that has detected major moraine forming events around the YD, the Erdalen Event and in some cases around the start of the Neoglaciation. The only exception would be our finding of a possible moraine forming event around the time of the 8.2 ka cold event. Although this period corresponds with a climate deterioration and a period of purported glacier expansion in Norway during the Finse Event (Nesje *et al.* 2008), very few moraines have been dated to this time, especially in northern Norway. Thus, we view this as a tentative hypothesis for future work to address. Nonetheless, we suggest that the preliminary moraine ages based on the Schmidt hammer dating are plausible and broadly consistent with previous work, and now discuss possible reasons for the anomalously old TCN ages, which appear much less plausible.

Comparing the TCN chronology to the regional deglaciation history, thinning of ice in Rotsunddalen could have feasibly occurred at ~16.3 ka (as indicated by TCN dating at the bedrock knoll), recording early deglaciation of the main ice sheet in northern Norway (cf. Fig. 16A). However, glacier retreat from outer to inner Sorbmevággi broadly between ~15.8 and 11.3 ka (or even approx. 13.7 and 10.1 ka based on the global production rate; Table 6) is inconsistent with numerous studies reporting ice extent in the region. First, the TCN ages imply complete deglaciation of the main part of Rotsunddalen, leaving a mountain glacier in Sorbmevággi, when regional evidence supports widespread ice-sheet coverage with a grounding line in the outer fjords (Fig. 16A). Second, the TCN chronology implies retreat of the Sorbmevággi glacier to the upper valley more than ~4500 years (or ~3500 years) before the HTM, when most ice masses reached their minimum

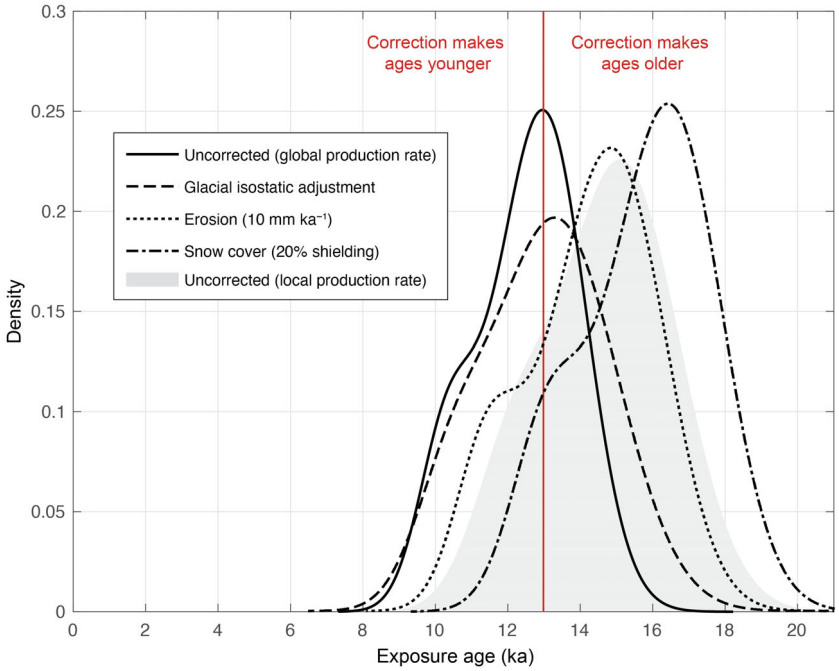

Fig. 17. Potential impacts on TCN ages. The curves represent the summed kernel density estimates for the Sorbmevággi and main part of Rotsunddalen TCN dataset, using different production rates and corrections. Exposure ages calculated with a global production rate (solid black line) are younger than those calculated using the local production rate (grey shaded area). The additional corrections (glacial isostatic adjustment, surface erosion, snow cover) only make the exposure ages older, as highlighted by the peaks of the dot/dashed curves (corrections) to the right of the peak of the solid curve (uncorrected). Corrections used iceTEA (Jones *et al.* 2019a), with age calculations done with the Cosmic Ray Exposure Program (Martin *et al.* 2017).

extents and probably disappeared (Fig. 16E), and more than ~6000 years (or ~5400 years) before Neoglaciation, when plateau glaciers reached their maximum Late Holocene extents (Fig. 16F). We therefore reject the TCN chronology and instead explore reasons why the ages may be anomalously old.

The successful application of TCN dating to reconstruct past glacier change around the world is based on the assumptions that a rock surface starts producing nuclides at a known rate when exposed by receding ice, and that nuclides can be lost through radioactive decay at a known rate (Schaefer *et al.* 2022). The nuclide concentration measured in a boulder surface is, however, dependent on several external factors that can result in outliers within a dataset (e.g. Heyman *et al.* 2011). To explain why all TCN-dated features are too old, we require a systematic influence on the samples at our site.

The first candidate is the production rate used to calculate exposure ages, as it has a near-identical influence across all samples within a dataset at a given study site. We used a local production rate based on two sites in northern Norway, but perhaps these sites provide an inaccurate rate, and instead a global average is more appropriate. The global production rate is higher than the local rate, resulting in lower nuclide concentrations and therefore younger exposure ages. However, as explained above, use of the global production rate still yields ages several thousand years too old when compared with the regional deglaciation history (Fig. 17). Further influences are therefore required to lower TCN ages, even if we assume that a global production rate is most accurate.

A second candidate is glacial isostatic adjustment, which can influence the production rate at a given site. As noted above, isostatic uplift owing to the deglaciation of the Fennoscandian Ice Sheet means that the production rate was probably lower at the time of exposure (lower elevation relative to today) but correcting for this effect makes the TCN ages older (Fig. 17).

A third candidate is snow cover, which can influence the production rate through partial shielding of the boulder surface from cosmic rays. We attempted to minimize the influence of snow cover, by sampling the top surfaces of large boulders, which would most likely be above ground snow and be more easily windswept, but snow cover cannot be ruled out. Nevertheless, any snow cover would lower the production rate, thereby making the TCN ages even older (Fig. 17).

A fourth candidate is subaerial erosion of the boulder surface, which can occur over time following exposure, resulting in a loss of nuclides. Any erosion means that the measured nuclide concentration underestimates the true concentration from the time of exposure (Balco 2020). Again, we attempted to minimize this

impact by sampling boulder surfaces with the least amount of postdepositional surface erosion. However, correcting for up to 10 mm ka^{-1} for this potential effect makes the TCN ages older, not younger (Fig. 17).

The fifth candidate is cosmogenic inheritance. Nuclides build up in a boulder surface during periods of exposure (e.g. interglacials, interstadials) and need to be fully removed by glacial erosion during periods of ice cover (e.g. glacials, stadials) to accurately record the most recent time of exposure. In cases where there has been insufficient erosion and a boulder has been re-deposited without complete removal of nuclides from a previous exposure period, the boulder 'inherits' nuclides with a resulting exposure age that overestimates the timing of recent exposure. We targeted boulders to sample that appeared eroded by ice (e.g. subrounded to subangular) to ideally eliminate the potential for any inheritance. However, erosive characteristics such as polished surfaces or glacial striae were not preserved on any of the samples. We propose that moraine SM5 probably had boulders with inheritance (Fig. 5E), possibly owing to insufficient glacial erosion in the upper part of the valley prior to glacier retreat, and it may be that this is a widespread issue across the study area.

The potential for cosmogenic inheritance varies spatially in mountainous regions. Inheritance is typically minimal in valleys, reflecting warm-based glaciation and the presence of erosive ice streams, and increases with elevation, reflecting cold-based glaciation of upland plateaus (Fabel *et al*. 2002; Briner *et al*. 2006). Measurement of modern glacial boulders from southern Norway showed that cosmogenic inheritance is near zero for material deposited by warm-based glaciers (Matthews *et al*. 2017). However, glacial erosion would probably be lower, and therefore inheritance higher, in areas away from such warm-based ice. Modelling of a cosmogenic nuclide dataset from western Norway highlighted that erosion occurred across plateau summits during glaciation, limiting the potential for inheritance (Andersen *et al*. 2018). However, erosion was both spatially and temporally variable beneath the Fennoscandian Ice Sheet, dependent on the thermodynamics (from cold- to warm-based ice) and the duration of ice cover (Kleman & Borgström 1994; Kleman *et al*. 1999; Rand & Goehring 2019; Patton *et al*. 2022). In peripheral areas of the ice sheet that experienced long ice-free periods with brief phases of (potentially cold-based) ice cover, cosmogenic nuclides can accumulate at depth in a rock surface. In such cases, >5 m of erosion is needed to avoid traces of inheritance in sampled boulders (Briner *et al*. 2016). Our study area is towards the periphery of the ice sheet, and the TCN ages could therefore reflect limited glacial erosion (<5 m).

In summary, we rule out factors related to the nuclide production rate, glacial isostatic adjustment, snow cover and surface erosion to explain TCN ages that are 'too old'. Instead, we propose that our TCN dataset records cosmogenic inheritance owing to insufficient glacial erosion.

Conclusions

This paper presents a new Holocene glacial chronology for the mountain glaciers of Rotsunddalen, Kåfjord Alps, in central Troms and Finnmark County, northern Norway, based on their glacial geomorphology and both relative and numerical dating methods. We hypothesize that the main ice-sheet margin was located at the head of the fjords and generally to the SE of the study area during the Younger Dryas, with large mountain glaciers, fed by plateau icefields depositing large moraines just beyond the confines of their subsidiary valleys between 12.1 and 10.6 ka. Continued recession of the main Fennoscandian Ice Sheet margin towards the SE led to the isolation of several large plateau icefields and outlet glaciers. In the subsidiary valleys of Hjemtverrdalen, Sorbmevággi and Goahtevággi, we hypothesize that moraines formed at around 10.2–9.2 ka, which we ascribe to the Erdalen Event, and 8.4–8.2 ka, which is broadly contemporaneous with the 8.2 ka cold event and might indicate that small maritime mountain glaciers were able to respond to short-term climatic perturbations. However, although this corresponds with the widely reported Finse Event in Scandinavia (Nesje *et al*. 2008), very few moraines have been dated to this time (especially in northern Norway) and we therefore view it as somewhat speculative and a key hypothesis for future work to test. During the Holocene Thermal Maximum (~6.6 to 6.3 ka) we hypothesize that most (if not all) glaciers in the region disappeared, but then regrew during the Neoglaciation and produced large moraines dated to around 4.7 ka that lie a few hundred metres distal to the prominent Little Ice Age moraines (previously dated to AD 1810s–1870s). Although early Neoglacial moraines have been reported at multiple sites in Scandinavia (Nesje *et al*. 2008; Nesje 2009), they tend to be located much further south of our study area and, given the limitations of our dating approach, this also warrants further investigation. Nonetheless, by combining our new moraine chronology with the extensive glacial geomorphological mapping of the region in Leigh *et al*. (2021), we are able to provide an updated ice-margin chronology for the Fennoscandian Ice Sheet and mountain glaciers from 14 ka to the present day.

Finally, despite their limitations, both Schmidt hammer dating and soil chronosequencing are shown to be potentially valuable techniques for assigning preliminary/relative ages to Holocene moraines in northern Norway. In contrast, we find that our TCN chronology is not consistent with the Schmidt hammer dating and the established regional deglaciation history and suggest that this reflects insufficient glacial erosion of the sampled boulders. This supports the notion that peripheral areas of former ice sheets, particularly at high

latitudes, are susceptible to cosmogenic inheritance. Valley glacier settings that receive large volumes of extra-glacial debris via rock slope failure which undergoes short and mostly passive travel distances are probably also problematic owing to minimal glacial erosion.

Acknowledgements. – The authors would like to thank the Editor, Stefan Winkler and an anonymous reviewer for their constructive comments during the peer review process. JRL was supported by a Natural Environment Research Council UK studentship (reference NE/L002590/1) and is grateful to Robert Leigh, James Linighan and Callum Pearson for fieldwork assistance. The terrestrial cosmogenic nuclide dating was funded by a UKRI National Environmental Isotope Facility grant (NEIF/2231/0320). The 2018 fieldwork was also supported by Lexus Norway, who provided a vehicle for JRL to use during fieldwork and by the Alpkit Foundation who provided monetary funding. The high-resolution Arctic DEMs were provided by the Polar Geospatial Centre under NSF-OPP awards 1043681, 1559691 and 1542736, and aerial orthophotographs were kindly provided by the Norwegian Mapping Authority (Kartverket). We also thank European Space Agency (ESA) and the US Geological Society for providing free satellite imagery and the Geological Survey of Norway for providing freely available geological data (made available by the Norwegian licence for public data). Prior glacier data as collated by the CryoClim project were also used, including glacier outlines downloaded directly from the Norwegian Water Resources and Energy Directorate website (https://www.nve.no/hydrology/glaciers/glacier-data/). Fennoscandian Ice Sheet margin positions and associated geochronological control data were sourced from the DATED-1 database and time-slice reconstruction map as editable GIS files (downloaded from http://doi.pangaea.de/10.1594/PANGAEA.848117).

Author contributions. – JRL, CRS and DJAE planned and designed the research. JRL led the data collection and fieldwork, supervised by CRS, DJAE, JRC and LMA. RSJ analysed and helped interpret the ^{10}Be dates. JRL wrote the first draft of the manuscript, with further input from CRS and RSJ. All authors helped interpret the data and commented on manuscript drafts.

Data availability statement. – The glacial geomorphological mapping is published in Leigh *et al*. (2021) and is also available on request to the corresponding author. The raw data from the Schmidt hammer dating, soil chronosequencing and terrestrial cosmogenic nuclide dating are available in the paper or from the corresponding author upon request.

References

Aa, A. R. & Sønstegaard, E. 2019: Early-Holocene glacier fluctuations of northern Grovabreen, western Norway. *Holocene 29*, 187–196.

Alley, R. B., Mayewski, P. A., Sowers, T., Stuiver, M., Taylor, K. C. & Clark, P. U. 1997: Holocene climatic instability: a prominent, widespread event 8200 yr ago. *Geology 25*, 483–486.

Andersen, B. G. 1965: Glacial chronology of Western Troms, North Norway. *Geological Society of America Special Papers 84*, 35–54.

Andersen, B. G. 1968: Glacial geology of Western Troms, North Norway. *Norges Geologiske Undersøkelse 256*, 160.

Andersen, B. G. 1980: The deglaciation of Norway after 10,000 B.P. *Boreas 9*, 211–216.

Andersen, J. L., Egholm, D. L., Knudsen, M. F., Linge, H., Jansen, J. D., Pedersen, V. K., Nielsen, S. B., Tikhomirov, D., Olsen, J., Fabel, D. & Xu, S. 2018: Widespread erosion on high plateaus during recent glaciations in Scandinavia. *Nature Communications 9*, 830, https://doi.org/10.1038/s41467-018-03280-2.

Andreassen, L. M., Elvehøy, H., Kjøllmoen, B. & Belart, M. C. 2020: Glacier change in Norway since the 1960s – an overview of mass balance, area, length and surface elevation changes. *Journal of Glaciology 66*, 31–328.

Andreassen, L. M., Kjøllmoen, B., Rasmussen, A., Melvold, K. & Nordli, Ø. 2012a: Langfjordjøkelen, a rapidly shrinking glacier in northern Norway. *Journal of Glaciology 58*, 581–593.

Andreassen, L. M., Nagy, T., Kjøllmoen, B. & Leigh, J. R. 2022: An inventory of Norway's glaciers and ice-marginal lakes from 2018–19 Sentinel-2 data. *Journal of Glaciology 68*, 1–22.

Andreassen, L. M., Winsvold, S. H., Paul, F. & Hausberg, J. E. 2012b: *Inventory of Norwegian Glaciers. NVE Report 38-2012*, 236 pp. Norwegian Water Resources and Energy Directorate, Oslo.

Applegate, P. J., Urban, N. M., Laabs, B. J., Keller, K. & Alley, R. B. 2010: Modeling the statistical distributions of cosmogenic exposure dates from moraines. *Geoscientific Model Development 3*, 293–307.

Augland, L. E., Andresem, A., Gasser, D. & Steltenpohl, M. G. 2014: Early Ordovician to Silurian evolution of exotic terranes in the Scandinavian Caledonides of the Ofoten–Troms area – terrane characterization and correlation based on new U–Pb zircon ages and Lu–Hf isotopic data. *Geological Society, London, Special Publications 390*, 655–678.

Bahr, D. B., Pfeffer, W. T., Sassolas, C. & Meier, M. F. 1998: Response time of glaciers as a function of size and mass balance: 1. Theory. *Journal of Geophysical Research – Solid Earth 103*, 9777–9782.

Bakke, J., Dahl, S. O. & Nesje, A. 2005a: Lateglacial and early Holocene palaeoclimatic reconstruction based on glacier fluctuations and equilibrium-line altitudes at northern Folgefonna, Hardanger, western Norway. *Journal of Quaternary Science 20*, 179–198.

Bakke, J., Dahl, S. O., Paasche, Ø., Løvlie, R. & Nesje, A. 2005b: Glacier fluctuations, equilibrium-line altitudes and palaeoclimate in Lyngen, northern Norway, during the Lateglacial and Holocene. *The Holocene 15*, 518–540.

Bakke, J., Dahl, S. O., Paasche, Ø., Simonsen, J. R., Kvisvik, B., Bakke, K. & Nesje, A. 2010: A complete record of Holocene glacier variability at Austre Okstindbreen, northern Norway: an integrated approach. *Quaternary Science Reviews 29*, 1246–1262.

Balascio, N. L. & Bradley, R. S. 2012: Evaluating Holocene climate change in northern Norway using sediment records from two contrasting lake systems. *Journal of Paleolimnology 48*, 259–273.

Balco, G. 2020: Glacier change and paleoclimate applications of cosmogenic-nuclide exposure dating. *Annual Review of Earth and Planetary Sciences 48*, 21–48.

Ballantyne, C. K. 1990: The Holocene glacial history of Lyngshalvoya, northern Norway: chronology and climatic implications. *Boreas 19*, 93–117.

Birkeland, P. W. 1978: Soil development as an indication of relative age of quaternary deposits, Baffin Island, N.W.T., Canada. *Arctic and Alpine Research 10*, 733–747.

Birkeland, P. W. 1999: *Soils and Geomorphology*. 386 pp. Oxford University Press, Oxford.

Birks, H. H. 1994: Late-glacial vegetational ecotones and climatic patterns in Western Norway. *Vegetation History and Archaeobotany 3*, 107–119.

Bjune, A. E., Bakke, J., Nesje, A. & Birks, H. J. B. 2005: Holocene mean July temperature and winter precipitation in western Norway inferred from palynological and glaciological lake-sediment proxies. *The Holocene 15*, 177–189.

Bondevik, S. & Mangerud, J. 2002: A calendar age estimate of a very late Younger Dryas ice sheet maximum in western Norway. *Quaternary Science Reviews 21*, 1661–1676.

Bridges, E. M. 1997: *World Soils*. 176 pp. Cambridge University Press, Cambridge.

Briner, J. P., Goehring, B. M., Mangerud, J. & Svendsen, J. I. 2016: The deep accumulation of 10Be at Utsira, southwestern Norway: implications for cosmogenic nuclide exposure dating in peripheral ice sheet landscapes. *Geophysical Research Letters 43*, 9121–9129.

Briner, J. P., Miller, G. H., Davis, P. T. & Finkel, R. C. 2006: Cosmogenic radionuclides from fiord landscapes support differential erosion by overriding ice sheets. *Geological Society of America Bulletin 118*, 406–420.

Buntley, G. J. & Westin, F. C. 1965: A comparative study of developmental colour in a Chestnut-Chernozem-Brunizem soil climosequence. *Soil Science Society of America Journal 29*, 579–582.

Coker-Dewey, J., Steltenpohl, M. G. & Andresen, A. 2000: Geology of western Ullsfjord, North Norway, with emphasis on the development of an inverted metamorphic gradient at the top of the Lyngen Nappe Complex. *Norwegian Journal of Geology 80*, 111–127.
Colman, S. M. 1981: Rock-weathering rates as functions time. *Quaternary Research 15*, 250–264.
Corner, G. D. 1980: Preboreal deglaciation chronology and marine limits of the Lyngen-Storfjord area, Troms, North Norway. *Boreas 9*, 239–249.
Dahl, S. O. & Nesje, A. 1994: Holocene glacier fluctuations at Hardangerjøkulen, central-southern Norway: a high-resolution composite chronology from lacustrine and terrestrial deposits. *The Holocene 4*, 269–277.
Dahl, S. O. & Nesje, A. 1996: A new approach to calculating Holocene winter precipitation by combining glacier equilibrium-line altitudes and pine-tree limits: a case study from Hardangerjøkulen, central southern Norway. *The Holocene 6*, 381–398.
Dahl, S. O., Nesje, A., Lie, Ø., Fjordheim, K. & Matthews, J. A. 2002: Timing, equilibrium-line altitudes and climatic implications of two early-Holocene glacier readvances during the Erdalen Event at Jostedalsbreen, western Norway. *The Holocene 12*, 17–25.
Day, M. J. 1977: Field assessment of rock hardness using the Schmidt hammer. *British Geomorphological Research Group Technical Bulletin 18*, 19–29.
Ellis, S. 1979: The identification of some Norwegian mountain soil types. *Norwegian Journal of Geology 33*, 205–212.
Evans, D. J. A. 1999: A soil chronosequence from Neoglacial moraines in western Norway. *Geografiska Annaler: Series A, Physical Geography 81*, 47–62.
Evans, D. J. A. 2008: Geomorphology: avalanches and moraines. *Nature Geoscience 1*, 493–494.
Evans, D. J. A., Rea, B. R., Hansom, J. D. & Whalley, W. B. 2002: Geomorphology and style of plateau icefield deglaciation in fjord terrains: the example of Troms-Finnmark, north Norway. *Journal of Quaternary Science 17*, 221–239.
Fabel, D., Stroeven, A. P., Harbor, J., Kleman, J., Elmore, D. & Fink, D. 2002: Landscape preservation under Fennoscandian ice sheets determined from *in situ* produced ^{10}Be and ^{26}Al. *Earth and Planetary Science Letters 201*, 397–406.
Fenton, C. R., Hermanns, R. L., Blikra, L. H., Kubik, P. W., Bryant, C., Niedermann, S., Meixner, A. & Goethals, M. M. 2011: Regional ^{10}Be production rate calibration for the past 12 ka deduced from the radiocarbon-dated Grøtlandsura and Russenes rock avalanches at 69 N, Norway. *Quaternary Geochronology 6*, 437–452.
Fitzpatrick, E. A. 1983: *Soils: Their Formation, Classification and Distribution*. 384 pp. Longman, London.
Forwick, M. & Vorren, T. O. 2002: Deglaciation history and post-glacial mass movements in Balsfjord, northern Norway. *Polar Research 21*, 259–266.
Geological Survey of Norway 2015: *Berggrunn: Nasjonal berggrunnsdatabase [National Bedrock Database]*. Available at: http://geo.ngu.no/kart/berggrunn/?lang=English (accessed 2.08.2018).
Giesen, R. H., Andreassen, L. M., Oerlemans, J. & Van den Broeke, M. R. 2014: Surface energy balance in the ablation zone of Langfjordjøkelen, an arctic, maritime glacier in northern Norway. *Journal of Glaciology 60*, 57–70.
Gjerde, M., Bakke, J., Vasskog, K., Nesje, A. & Hormes, A. 2016: Holocene glacier variability and Neoglacial hydroclimate at Ålfotbreen, western Norway. *Quaternary Science Reviews 133*, 28–47.
Griffey, N. J. & Whalley, W. B. 1979: A rock glacier and moraine-ridge complex, Lyngen Peninsula, north Norway. *Norwegian Journal of Geology 33*, 117–124.
Griffey, N. J. & Worsley, P. 1978: The pattern of Neoglacial glacier variations in the Okstindan region of northern Norway during the last three millennia. *Boreas 7*, 1–17.
Grove, J. M. 2001: The initiation of the "Little Ice Age" in regions round the North Atlantic. *Climatic Change 48*, 53–82.
Grove, J. M. 2004: *Little Ice Ages: Ancient and Modern*. 817 pp. Routledge, London.
Heyman, J., Stroeven, A. P., Harbor, J. M. & Caffee, M. W. 2011: Too young or too old: evaluating cosmogenic exposure dating based on an analysis of compiled boulder exposure ages. *Earth and Planetary Science Letters 302*, 71–80.
Holmes, G. W. & Andersen, B. G. 1964: Glacial chronology of Ullsfjord, northern Norway. *United States Geological Survey Professional Paper D 475*, 159–163.
Hughes, A. L. C., Gyllencreutz, R., Lohne, Ø., Mangerud, J. & Svendsen, J. I. 2016: The last Eurasian ice sheets – a chronological database and time-slice reconstruction, DATED-1. *Boreas 45*, 1–45.
Ivy-Ochs, S., Kerschner, H., Maisch, M., Christl, M., Kubik, P. W. & Schlüchter, C. 2009: Latest Pleistocene and Holocene glacier variations in the European Alps. *Quaternary Science Reviews 28*, 2137–2149.
Jansen, H. L., Dahl, S. O., Linge, H., Bakke, J., Nielsen, P. R. & Kvisvik, B. C. 2023: Palaeoclimatic and regional implications of Older Dryas and Younger Dryas local glacier activity in the low-Arctic valley Finnkongdalen, Andøya, northern Norway. *Boreas 52*, 168–193.
Jansen, H. L., Simonsen, J. R., Dahl, S. O., Bakke, J. & Nielsen, P. R. 2016: Holocene glacier and climate fluctuations of the maritime ice cap Høgtuvbreen, northern Norway. *Holocene 26*, 736–755.
Jóhannesson, T., Raymond, C. F. & Waddington, E. D. 1989: A simple method for determining the response time of glaciers. *In* Oerlemans, J. (ed.): *Glacier Fluctuations and Climatic Change*, 334–352. Springer, Dordrecht.
Jones, R. S., Small, D., Cahill, N., Bentley, M. J. & Whitehouse, P. L. 2019: iceTEA: tools for plotting and analysing cosmogenic-nuclide surface-exposure data from former ice margins. *Quaternary Geochronology 51*, 72–86.
Jones, R. S., Whitehouse, P. L., Bentley, M. J., Small, D. & Dalton, A. S. 2019: Impact of glacial isostatic adjustment on cosmogenic surface-exposure dating. *Quaternary Science Reviews 212*, 206–212.
Karlén, W. 1988: Scandinavian glacial and climatic fluctuations during the Holocene. *Quaternary Science Reviews 7*, 199–209.
Karlén, W. & Kuylenstierna, J. 1996: On solar forcing of Holocene climate: evidence from Scandinavia. *Holocene 6*, 359–365.
Kleman, J. & Borgström, I. 1994: Glacial landforms indicative of a partly frozen bed. *Journal of Glaciology 40*, 255–264.
Kleman, J., Hättestrand, C. & Clarhäll, A. 1999: Zooming in on frozen-bed patches: scale-dependent controls on Fennoscandian ice sheet basal thermal zonation. *Annals of Glaciology 28*, 189–194.
Klingbjer, P., Brown, I. A. & Holmlund, P. 2005: Identification of climate controls on the dynamic behaviour of the subarctic glacier Salajekna, northern Scandinavia. *Geografiska Annaler: Series A, Physical Geography 87*, 215–229.
Kverndal, A.-I. & Sollid, J. L. 1993: Late Weichselian glaciation and deglaciation in northeastern Troms, northern Norway. *Norwegian Journal of Geology 47*, 163–177.
Kvisvik, B. C., Paasche, Ø. & Dahl, S. O. 2015: Holocene cirque glacier activity in Rondane, southern Norway. *Geomorphology 246*, 433–444.
Lauritzen, S. E. & Lundberg, J. 1999: Calibration of the speleothem delta function: an absolute temperature record for the Holocene in northern Norway. *The Holocene 9*, 659–669.
Leigh, J. R., Evans, D. J. A., Stokes, C. R., Andreassen, L. M. & Carr, R. J. 2021: Glacial and periglacial geomorphology of central Troms and Finnmark county, Arctic Norway. *Journal of Maps 17*, 348–366.
Leigh, J. R., Stokes, C. R., Evans, D. J. A. & Andreassen, L. M. 2020: Timing of Little Ice Age maxima and subsequent glacier retreat in northern Troms and western Finnmark, northern Norway. *Arctic, Antarctic, and Alpine Research 52*, 281–311.
Lifton, N., Sato, T. & Dunai, T. J. 2014: Scaling *in situ* cosmogenic nuclide production rates using analytical approximations to atmospheric cosmic-ray fluxes. *Earth and Planetary Science Letters 386*, 149–160.
Lindahl, I., Stevens, B. P. J. & Zwaan, K. B. 2005: The geology of the Váddás area, Troms: a key to our understanding of the Upper Allochthon in the Caledonides of northern Norway. *Norges Geologiske Undersøkelse 445*, 5–43.
Lohne, Ø. S., Mangerud, J. & Svendsen, J. I. 2012: Timing of the Younger Dryas glacial maximum in Western Norway. *Journal of Quaternary Science 27*, 81–88.
Mangerud, J., Aarseth, I., Hughes, A. L. C., Lohne, Ø., Skår, K., Sønstergaard, E. & Svendsen, J. I. 2016: A major re-growth of the

Scandinavian Ice Sheet in western Norway during Allerød-Younger Dryas. *Quaternary Science Reviews 132*, 175–205.
Marthinussen, M. 1962: ^{14}C-datings referring to shore lines, transgressions, and glacial substages in northern Norway. *Norsk Geologisk Undersøkelse 215*, 37–67.
Martin, L. C. P., Blard, P. H., Balco, G., Lavé, J., Delunel, R., Lifton, N. & Laurent, V. 2017: The CREp program and the ICE-D production rate calibration database: a fully parameterizable and updated online tool to compute cosmic-ray exposure ages. *Quaternary Geochronology 38*, 25–49.
Matthews, J. A. 1991: The late Neoglacial ('Little Ice Age') glacier maximum in southern Norway: new 14C-dating evidence and climatic implications. *The Holocene 1*, 219–233.
Matthews, J. A. & Dresser, P. Q. 2008: Holocene glacier variation chronology of the Smørstabbtindan massif, Jotunheimen, southern Norway, and the recognition of century- to millennial-scale European Neoglacial Events. *Holocene 18*, 181–201.
Matthews, J. A. & Winkler, S. 2011: Schmidt-hammer exposure-age dating (SHD): application to early Holocene moraines and a reappraisal of the reliability of terrestrial cosmogenic-nuclide dating (TCND) at Austanbotnbreen, Jotunheimen, Norway. *Boreas 40*, 256–270.
Matthews, J. A. & Winkler, S. 2022: Schmidt-hammer exposure-age dating: a review of principles and practice. *Earth-Science Reviews 239*, 104038, https://doi.org/10.1016/j.earscirev.2022.104038.
Matthews, J. A., Berrisford, M. S., Dresser, P. Q., Nesje, A., Dahl, S. O., Bjune, A. E., Bakke, J., John, H., Birks, B., Lie, Ø., Dumayne-Peaty, L. & Barnett, C. 2005: Holocene glacier history of Bjørnbreen and climatic reconstruction in central Jotunheimen, Norway, based on proximal glaciofluvial stream-bank mires. *Quaternary Science Reviews 24*, 67–90.
Matthews, J. A., Shakesby, R. A. & Fabel, D. 2017: Very low inheritance in cosmogenic surface exposure ages of glacial deposits: a field experiment from two Norwegian glacier forelands. *The Holocene 27*, 1406–1414.
Matthews, J. A., Shakesby, R. A., Schnabel, C. & Freeman, S. 2008: Cosmogenic 10Be and 26Al ages of Holocene moraines in southern Norway I: testing the method and confirmation of the date of the Erdalen Event (c. 10 ka) at its type-site. *Holocene 18*, 1155–1164.
McCarroll, D. 1989: Potential and limitations of the Schmidt hammer for relative-age dating: field tests on Neoglacial moraines, Jotunheim, southern Norway. *Arctic and Alpine Research 21*, 268–275.
McCarroll, D. & Ware, M. 1989: The variability of soil development on Preboreal moraine ridge crests, Breiseterdalen, southern Norway. *Norsk Geografisk Tidsskrift - Norwegian Journal of Geography 43*, 31–36.
Mendelová, M., Hein, A. S., Rodes, A., & Xu, S. 2020: Extensive mountain glaciation in central Patagonia during Marine Isotope Stage 5. *Quaternary Science Reviews 227*, 105996.
Nesje, A. 2009: Latest Pleistocene and Holocene alpine glacier fluctuations in Scandinavia. *Quaternary Science Reviews 28*, 2119–2136.
Nesje, A. & Dahl, S. O. 2001: The Greenland 8200 cal. yr BP event detected in loss-on-ignition profiles in Norwegian lacustrine sediment sequences. *Journal of Quaternary Science 16*, 155–166.
Nesje, A. & Kvamme, M. 1991: Holocene glacier and climate variations in western Norway: evidence for early or early Holocene glacier demise and multiple Neoglacial events. *Geology 19*, 610–612.
Nesje, A., Bakke, J., Dahl, S. O., Lie, Ø. & Matthews, J. A. 2008: Norwegian mountain glaciers in the past, present and future. *Global and Planetary Change 60*, 10–27.
Nesje, A., Bjune, A. E., Bakke, J., Dahl, S. O., Lie, Ø. & Birks, H. J. B. 2006: Holocene palaeoclimate reconstructions at Vanndalsvatnet, western Norway, with particular reference to the 8200 cal. yr BP event. *Holocene 16*, 717–729.
Nesje, A., Kvamme, M., Rye, N. & Løvlie, R. 1991: Holocene glacial and climate history of the Jostedalsbreen region, Western Norway; evidence from lake sediments and terrestrial deposits. *Quaternary Science Reviews 10*, 87–114.
Nesje, A., Lie, Ø. & Dahl, S. O. 2000: Is the North Atlantic Oscillation reflected in Scandinavian glacier mass balance records? *Journal of Quaternary Science 15*, 587–601.
Norwegian Mapping Authority n.d.: Available at: https://www.norgeibilder.no/.
Nydal, E. 1960: Trondheim natural radiocarbon measurements II. *Radiocarbon 2*, 82–96.
Oerlemans, J. 2005: Extracting a climate signal from 169 glacier records. *Science 308*, 675–677.
Oerlemans, J. 2007: Estimating response times of Vadret da Morteratsch, Vadret da Palü, Briksdalsbreen and Nigardsbreen from their length records. *Journal of Glaciology 53*, 357–362.
Paasche, Ø., Dahl, S. O., Bakke, J., Løvlie, R. & Nesje, A. 2007: Cirque glacier activity in Arctic Norway during the last deglaciation. *Quaternary Research 68*, 387–399.
Palacios, D., Rodríguez-Mena, M., Fernández-Fernández, J. M., Schimmelpfennig, I., Tanarro, L. M., Zamorano, J. J., Andrés, N., Úbeda, J., Sæmundsson, Þ., Brynjólfsson, S., Oliva, M. & A.S.T.E.R. Team 2021: Reversible glacial-periglacial transition in response to climate changes and paraglacial dynamics: a case study from Héðinsdalsjökull (northern Iceland). *Geomorphology 388*, 107787, https://doi.org/10.1016/j.geomorph.2021.107787.
Park, H.-S., Kim, S.-J., Stewart, A. L., Son, S.-W. & Seo, K.-H. 2019: Mid-Holocene northern hemisphere warming driven by Arctic amplification. *Science Advances 5*, eaax8203, https://doi.org/10.1126/sciadv.aax8203.
Patton, H., Hubbard, A., Heyman, J., Alexandropoulou, N., Lasabuda, A. P., Stroeven, A. P., Hall, A. M., Winsborrow, M., Sugden, D. E., Kleman, J. & Andreassen, K. 2022: The extreme yet transient nature of glacial erosion. *Nature Communications 13*, 7377, https://doi.org/10.1038/s41467-022-35072-0.
Paus, A., Halflidason, H., Routh, J., Naafs, B. D. A. & Thoen, M. W. 2019: Environmental responses to the 9.7 and 8.2 cold events at two ecotonal sites in the Dovre mountains, mid-Norway. *Quaternary Science Reviews 205*, 45–61.
Paus, A., Velle, G., Larsen, J., Nesje, A. & Lie, Ø. 2006: Lateglacial nunataks in central Scandinavia: Biostratigraphical evidence for ice thickness from Lake Flåfattjønn, Tynset, Norway. *Quaternary Science Reviews 25*, 1228–1246.
Placek, A. & Mignon, P. 2007: Rock-landform relationships in the Sudetes in the light of rock strength assessment using Schmidt hammer. *Geomorphological Variations 1*, 287–311.
Plassen, L. & Vorren, T. O. 2003: Sedimentary processes and the environment during deglaciation of a fjord basin in Ullsfjorden, North Norway. *Norwegian Journal of Geology 83*, 23–36.
Porter, C., Morin, P., Howat, I., Noh, M., Bates, B., Peterman, K., Keesey, D., Schlenk, M., Gardiner, J. & Tomko, K. 2018: *ArcticDEM*. Polar Geospatial Center. Available at https://www.pgc.umn.edu/.
Rand, C. & Goehring, B. M. 2019: The distribution and magnitude of subglacial erosion on millennial timescales at Engabreen, Norway. *Annals of Glaciology 60*, 73–81.
Randal, B. A. O. 1971: The igneous rocks of the Lyngen Peninsula, Troms, Norway. *Norges Geologiske Undersøkelse 269*, 143–146.
Rea, B. R. & Evans, D. J. A. 2007: Quantifying climate and glacier mass balance in north Norway during the Younger Dryas. *Palaeogeography, Palaeoclimatology, Palaeoecology 246*, 307–330.
Renssen, H., Seppä, H., Crosta, X., Goose, H. & Roche, D. M. 2012: Global characterization of the Holocene Thermal Maximum. *Quaternary Science Reviews 48*, 7–19.
Renssen, H., Seppä, H., Heiri, O., Roche, D. M., Goose, H. & Fichefet, T. 2009: The spatial and temporal complexity of the Holocene Thermal Maximum. *Nature Geoscience 2*, 411–414.
Risebrobakken, B., Jansen, E., Andersson, C., Mjelde, E. & Hevrøy, K. 2003: A high-resolution study of Holocene paleoclimatic and paleoceanographic changes in the Nordic Seas. *Paleoceanography 18*, 1017, https://doi.org/10.1029/2002PA000764.
Roe, G. H., Baker, M. B. & Herla, F. 2017: Centennial glacier retreat as categorical evidence of regional climate change. *Nature Geoscience 10*, 95–99.
Rohling, E. E. & Pälike, H. 2005: Centennial-scale climate cooling with a sudden cold event around 8,200 years ago. *Nature 434*, 975–979.
Romundset, A., Akçar, N., Fredin, O., Tikhomirov, D., Reber, R., Vockenhuber, C., Christl, M. & Schlüchter, C. 2017: Lateglacial retreat chronology of the Scandinavian Ice Sheet in Finnmark,

northern Norway, reconstructed from surface exposure dating of major end moraines. *Quaternary Science Reviews 177*, 130–144.
Rosqvist, G. C., Jonsson, C., Yam, R., Karlén, W. & Shemesh, A. 2004: Diatom oxygen isotopes in pro-glacial lake sediments from northern Sweden: a 5000 year record of atmospheric circulation. *Quaternary Science Reviews 23*, 851–859.
Rosqvist, G. C. & Østrem, G. 1989: The sensitivity of a small icecap to climatic fluctuations. *Geografiska Annaler: Series A, Physical Geography 71*, 99–103.
Rounce, D. R., Hock, R., Maussion, F., Huggonnet, R., Kochtitzky, W., Huss, M., Berthier, E., Brinkerhoff, D., Compagno, L., Copland, L., Farinotti, D., Menounos, B. & McNabb, R. W. 2023: Global glacier change in the 21st century: every increase in temperature matters. *Science 379*, 78–83.
Rouyet, L., Lilleøren, K. S., Böhme, M., Vick, L. M., Delaloye, R., Etzelmüller, B., Lauknes, T. R., Larsen, Y. & Bilkra, L. H. 2021: Regional morpho-kinematic inventory of slope movements in northern Norway. *Frontiers in Earth Science 9*, 681088, https://doi.org/10.3389/feart.2021.681088.
Schaefer, J. M., Codilean, A. T., Willenbring, J. K., Lu, Z. T., Keisling, B., Fülöp, R. H. & Val, P. 2022: Cosmogenic nuclide techniques. *Nature Reviews Methods Primers 2*, 19, https://doi.org/10.1038/s43586-022-00111-z.
Seierstad, J., Nesje, A., Dahl, S. O. & Simonsen, J. R. 2002: Holocene glacier fluctuations of Grovabreen and Holocene snow-avalanche activity reconstructed from lake sediments in Grøningstølsvatnet, western Norway. *Holocene 12*, 211–222.
Seppä, H. & Birks, H. J. B. 2002: Holocene climate reconstructions from the Fennoscandian tree-line area based on pollen data from Toskaljavri. *Quaternary Research 57*, 191–199.
Seppä, H., Hammarlund, D. & Antonsson, K. 2005: Low-frequency and high-frequency changes in temperature and effective humidity during the Holocene in south-central Sweden: implications for atmospheric and oceanic forcings of climate. *Climate Dynamics 25*, 285–297.
Serreze, M. C. & Barry, R. G. 2011: Processes and impacts of Arctic amplification: a research synthesis. *Global and Planetary Change 77*, 85–96.
Shakesby, R. A., Matthews, J. A., Karlén, W. & Los, S. O. 2011: The Schmidt hammer as a Holocene calibrated-age dating technique: testing the form of the R-value-age relationship and defining the predicted-age errors. *Holocene 21*, 615–628.
Shakesby, R. A., Matthews, J. A. & Owen, G. 2006: The Schmidt hammer as a relative-age dating tool and its potential for calibrated-age dating in Holocene glaciated environments. *Quaternary Science Reviews 25*, 2846–2867.
Sollid, J. L., Andersen, S., Hamre, N., Kjeldsen, O., Salvigsen, O., Sturød, S., Tveitå, T. & Wilhelmsen, A. 1973: Deglaciation of Finnmark, North Norway. *Norwegian Journal of Geology 27*, 233–325.
Solomina, O. N., Bradley, R. S., Jomelli, V., Geirsdottir, A., Kaufman, D. S., Koch, J., McKay, N. P., Masiokas, M., Miller, G., Nesje, A., Nicolussi, K., Owen, L. A., Putnam, A. E., Wanner, H., Wiles, G. & Yang, B. 2016: Glacier fluctuations during the past 2000 years. *Quaternary Science Reviews 149*, 61–90.
Stokes, C. R., Andreassen, L. M., Champion, M. R. & Corner, G. D. 2018: Widespread and accelerating glacier retreat on the Lyngen Peninsula, northern Norway, since their "Little Ice Age" maximum. *Journal of Glaciology 64*, 100–118.
Stokes, C. R., Corner, G. D., Winsborrow, M. C. M., Husum, K. & Andreassen, K. 2014: Asynchronous response of marine-terminating outlet glaciers during deglaciation of the Fennoscandian ice sheet. *Geology 42*, 455–458.
Stroeven, A. P., Hättestrand, C., Kleman, J., Heyman, J., Fabel, D., Fredin, O., Goodfellow, B. W., Harbor, J. M., Jansen, J. D., Olsen, L., Caffee, M. W., Fink, D., Lundqvist, J., Rosqvist, G. C., Strömberg, B. & Jansson, K. N. 2016: Deglaciation of Fennoscandia. *Quaternary Science Reviews 147*, 91–121.
Tanarro, L. M., Palacios, D., Fernández-Fernández, J. M., Andrés, N., Oliva, M., Rodríguez-Mena, M., Schimmelpfennigd, I., Brynjólfsson, S., Sæmundsson, T., Zamorano, J. J., Úbeda, J. & ASTER Team 2021: Origins of the divergent evolution of mountain glaciers during deglaciation: Hofsdalur cirques, Northern Iceland. *Quaternary Science Reviews 273*, 107248, https://doi.org/10.1016/j.quascirev.2021.107248.
Tomkins, M. D., Huck, J. J., Dortch, J. M., Hughes, P. D., Kirkbridge, M. P. & Barr, I. D. 2018: Schmidt Hammer exposure dating (SHED): calibration procedures, new exposure age data and an online calculator. *Quaternary Geochronology 44*, 55–62.
Turner, J. & Marshall, G. J. 2011: *Climate Change in the Polar Regions*. 434 pp. Cambridge University Press, Cambridge.
Vacco, D. A., Alley, R. B. & Pollard, D. 2010: Glacial advance and stagnation caused by rock avalanches. *Earth and Planetary Science Letters 294*, 123–130.
Vorren, T. O. & Plassen, L. 2002: Deglaciation and palaeoclimate of the Andfjord-Vågsfjord area, North Norway. *Boreas 31*, 97–125.
Weber, P., Lovell, H., Andreassen, L. M. & Boston, C. M. 2020: Reconstructing the Little Ice Age extent of Langfjordjøkelen, Arctic mainland Norway, as a baseline for assessing centennial-scale icefield recession. *Polar Research 39*, 1–21.
Whalley, W. B. 1976: A rock glacier and its relation to the mass balance of corrie glaciers, Strupbreen, Troms, Norway. *Norwegian Journal of Geology 30*, 51–55.
Whalley, W. B. 1992: A rock glacier in south Ellendalen, Lyngen Alps, Troms. *Norwegian Journal of Geology 46*, 29–31.
Wilson, P., Linge, H., Matthews, J. A., Mourne, R. W. & Olsen, J. 2019: Comparative numerical surface exposure-age dating (^{10}Be and Schmidt hammer) of an early-Holocene rock avalanche at Alstadfjellet, Valldalen, southern Norway. *Geografiska Annaler: Series A, Physical Geography 101*, 293–309.
Winkler, S. 2003: A new interpretation of the date of the "Little Ice Age" glacier maximum at Svartisen and Okstindan, northern Norway. *The Holocene 13*, 83–95.
Winkler, S. 2014: Investigation of late-Holocene moraines in the western Southern Alps, New Zealand, applying Schmidt-hammer exposure-age dating. *The Holocene 24*, 48–66.
Wittmeier, H. E., Bakke, J., Vasskog, K. & Trachsel, M. 2015: Reconstructing Holocene glacier activity at Langfjordjøkelen, Arctic Norway, using multi-proxy fingerprinting of distal glacier-fed lake sediments. *Quaternary Science Reviews 114*, 78–99.
Ye, S., Cuzzone, J. K., Marcott, S. A., Licciardi, J. M., Ward, D. J., Heyman, J. & Quinn, D. P. 2023: A quantitative assessment of snow shielding effects on surface exposure dating from a western North American ^{10}Be data compilation. *Quaternary Geochronology 76*, 101440, https://doi.org/10.1016/j.quageo.2023.101440.
Zemp, M. and 38 others. 2015: Historically unprecedented global glacier decline in the early 21st century. *Journal of Glaciology 61*, 745–762.
Zemp, M., Huss, M., Thibert, E., Eckert, N., McNabb, R., Huber, J., Baradun, M., Machguth, H., Nussbaumer, S. U., Gärtner-Roer, I., Thomson, L., Paul, F., Maussion, F., Kutuzov, S. & Cogley, J. G. 2019: Global glacier mass changes and their contributions to sea-level rise from 1961 to 2016. *Nature 568*, 382–386.

Supporting Information

Additional Supporting Information to this article is available at http://www.boreas.dk.

Fig. S1. Mean *R*-value and ±95% confidence intervals for each boulder (grey box and line) and mean *R*-value from all boulders on a feature (black box and line) from each moraine sampled in Strupskardet.

Fig. S2. Mean *R*-value and ±95% confidence intervals for each boulder (grey box and line) and mean *R*-value from all boulders on a feature (black box and line) from each moraine in (A) Sorbmevágg and (B) Hjemtverrdalen.